

ChemistrySelect

Chemistry
Europe
European Chemical
Societies Publishing

Editorial Board

Chairs



Didier Astruc is a full professor of chemistry at the Université Bordeaux I. He is known for his work on "electron-reservoir" complexes, dendritic molecular batteries, green catalysis, and sensors.



Hélène Lebel is a professor of chemistry at the Université de Montréal. Her research is focused on catalysis in synthetic organic chemistry, pharmacologically useful molecules, and multicatalytic processes that mimic biosynthesis in living cells.



An-Hui Lu is a professor of chemistry at the State Key Laboratory of Fine Chemicals, Dalian University of Technology. His research interests include the synthesis of porous materials for heterogeneous catalysis, adsorption, energy storage and conversion.







Members

- Raed Abu-Reziq** (The Hebrew University of Jerusalem)
- Marius Andruh** (Universitatea din București)
- Ülkü Anık** (Muğla Sıtkı Koçman University)
- Viktorya Aviyente** (Boğaziçi University)
- R. Tom Baker** (University of Ottawa)
- Thomas Baumgartner** (York University)
- Michael J. Bojdys** (Humboldt-Universität zu Berlin)
- Azzedine Bousseksou** (Laboratoire de Chimie de Coordination, CNRS)
- Carlos D. Brondino** (Universidad Nacional del Litoral)
- Juraj Bujdak** (Univerzita Komenského v Bratislave)
- Jianfeng Cai** (University of South Florida)
- Luigi Cavallo** (King Abdullah University of Science and Technology)
- Jiří Čejka** (Akademie věd České republiky)
- Hugo E. Cerecetto** (Universidad de la República)
- Banglin Chen** (University of Texas at San Antonio)
- Sheng Dai** (Oak Ridge National Laboratory)
- Jiří Damborský** (Masarykova univerzita)
- Aditi Das** (University of Illinois)
- Fabian M. Dayrit** (Ateneo de Manila University)
- Da-Ming Du** (Beijing Institute of Technology)
- Charl Faul** (University of Bristol)
- Shin-ichi Fukuzawa** (Chuo University)
- François Gabbai** (Texas A&M University)
- Miran Gaberšček** (Kemijski inštitut Ljubljana Slovenija)
- Karol Grela** (University of Warsaw)
- Daniel Gryko** (Polska Akademia Nauk)
- Michael Harmata** (University of Missouri-Columbia)
- Christian Heinis** (École Polytechnique Fédérale de Lausanne)
- Dennis Hettterscheid** (Universiteit Leiden)

-  Yong-Sheng **Hu** (Institute of Physics, CAS)
-  Reuben **Hwu** (National Tsing Hua University)
-  Josef **Jampilek** (Univerzita Komenského v Bratislave)
-  Hye-Young **Jang** (Ajou University)
-  Knud **Jensen** (Københavns Universitet)
-  Deborah **Jones** (L'Institut de Chimie Moléculaire et des Matériaux)
-  Babak **Karimi** (Institute for Advanced Studies in Basic Sciences)
-  Uwe **Karst** (Westfälische Wilhelms-Universität Münster)
-  Henryk **Kozłowski** (Uniwersytet Wrocławski)
-  Yuehe **Lin** (Washington State University)
-  Chenghui **Liu** (Shaanxi Normal University)
-  Chun-yan **Liu** (Technical Institute of Physics and Chemistry, CAS)
-  Gregor **Mali** (Kemjski inštitut Ljubljana Slovenija)
-  Jose L. **Marco-Contelles** (Química Orgánica General del CSIQ)
-  Sherri **McFarland** (University of North Carolina at Greensboro)
-  Gabriel **Merino** (Centro de Investigación y de Estudios Avanzados Unidad Mérida)
-  Kenji **Miyatake** (University of Yamanashi)
-  Yirong **Mo** (Western Michigan University)
-  Thomas E. **Müller** (RWTH Aachen)
-  Samir H. **Mushrif** (University of Alberta)
-  Srinivasan **Natarajan** (Indian Institute of Science, Bangalore)
-  Georgii I. **Nikonov** (Brock University)
-  Turan **Öztürk** (Istanbul Technical University)
-  Mario **Pagliaro** (Istituto per lo Studio dei Materiali Nanostrutturati del CNR, Palermo)
-  Maurizio **Peruzzini** (Dipartimento Scienze Chimiche e Technologie del CNR)
-  Teresa M. V. D. **Pinho e Melo** (Universidade De Coimbra)
-  Uwe **Pischel** (Universidad de Huelva)
-  László **Poppe** (Budapesti Műszaki és Gazdaságtudományi Egyetem)
-  Vinich **Promarak** (Vidyasirimedhi Institute of Science and Technology)
-  Rasmita **Raval** (University of Liverpool)
-  Leni **Ritmaleni** (Universitas Gadjah Mada)
-  Johan **Rosengren** (The University of Queensland)
-  Liane Marcia **Rossi** (Universidade de São Paulo)
-  Agnieszka **Ruppert** (Politechnika Łódzka)
-  Ulrich **Schatzschneider** (Julius-Maximilians-Universität Würzburg)
-  YuYe Jay **Tong** (Georgetown University)
-  Konstantinos S. **Triantafyllidis** (Aristotle University of Thessaloniki)
-  Andrew **Tsotinis** (University of Athens)
-  Xincheng **Wang** (Fuzhou University)
-  Gang **Wu** (University at Buffalo)

Former Members

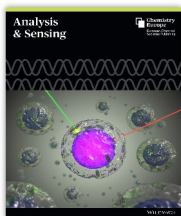
-  Gaoquan **Shi** (Tsinghua University)

-  [Submit a Manuscript](#)
-  [Browse free sample issue](#)
-  [Get content alerts](#)
-  [Subscribe to this journal](#)

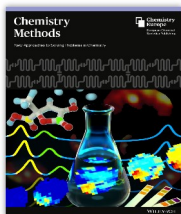
More from this journal

- [Reviews](#)
- [Editorials](#)
- [Video Abstracts](#)

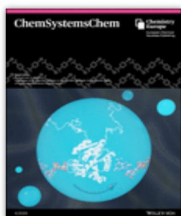




NEW JOURNAL:
Analysis & Sensing
Accepting submissions now.



NEW JOURNAL:
Chemistry—Methods
Accepting submissions now.



ISSUE
Volume 2, Issue 4
July 2020



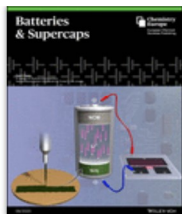
ISSUE
Volume 26, Issue 43
Pages: 9403-9651
August 3, 2020



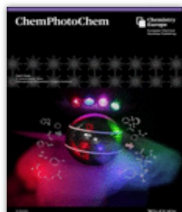
ISSUE
Volume 9, Issue 8
Pages: 793-817
August 2020



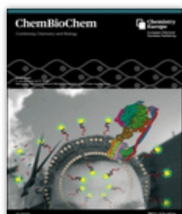
ISSUE
Volume 5, Issue 29
Pages: 8881-9312
August 7, 2020



ISSUE
Volume 3, Issue 8
Pages: 668-788
August 2020



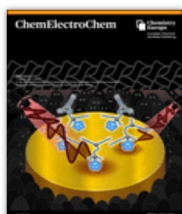
ISSUE
Volume 4, Issue 7
Pages: 451-534
July 2020



ISSUE
Volume 21, Issue 15
Pages: 2086-2224
August 3, 2020



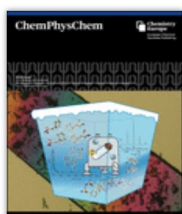
ISSUE
Volume 12, Issue 14
Pages: 3598-3792
July 21, 2020



ISSUE
Volume 7, Issue 15
Pages: 3168-3323
August 3, 2020



ISSUE
Volume 15, Issue 15
Pages: 1372-1496
August 5, 2020



ISSUE
Volume 21, Issue 15
Pages: 1617-1736
August 4, 2020



ISSUE

Volume 85, Issue 8
Pages: 1612-1709
August 2020



ISSUE

Volume 13, Issue 14
Pages: 3539-3725
July 22, 2020



ISSUE

Volume 2020, Issue 29
Pages: 2767-2849
August 9, 2020



ISSUE

Volume 2020, Issue 29
Pages: 4433-4638
August 9, 2020



[ChemistryViews.org](https://chemistryviews.org) Home

Mn-Catalyzed Transfer Hydrogenation of Esters

06 Aug 2020

Ester reduction using ethanol instead of hydrogen

90th Anniversary: Death of Joseph Achille Le Bel

06 Aug 2020

French chemist and co-discoverer of the basic concepts of organic stereochemistry

Giant Mo₂₄₀ Dodecahedra

05 Aug 2020

Polymolybdate cage with pentagonal openings

Oxygen-Stable State of [FeFe] Hydrogenase Studied

05 Aug 2020

A sulfur ligand causes oxygen stability

Nursing, Gut Bacteria, and the Immune System – Part 2

04 Aug 2020

What are human milk oligosaccharides (HMO)?

ACES Asian Chemical Editorial Society



ISSUE

Volume 15, Issue 15
The Chemistry of 2D Materials Membranes

Pages: 2239-2378
August 3, 2020



ISSUE

Volume 9, Issue 7
Pages: 967-1086
July 2020



ISSUE

Volume 6, Issue 7
Pages: 996-1135
July 2020

© 2020 WILEY-VCH Verlag GmbH & Co. KGaA, Weinheim

About Wiley Online Library

[Privacy Policy](#)
[Terms of Use](#)
[Cookies](#)
[Accessibility](#)

[Help & Support](#)

[Contact Us](#)

[Opportunities](#)

Subscription Agents
Advertisers & Corporate Partners

Connect with Wiley

The Wiley Network
Wiley Press Room

Copyright © 1999-2020 John Wiley & Sons, Inc. All rights reserved

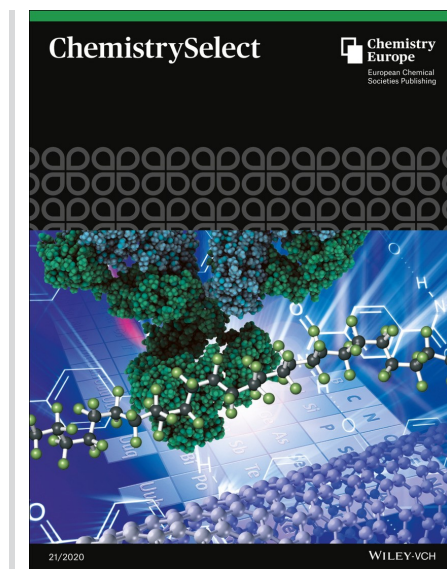
ChemistrySelect**Chemistry
Europe**
European Chemical
Societies Publishing**Volume 5, Issue 21**

Pages: 6236-6525

June 8, 2020

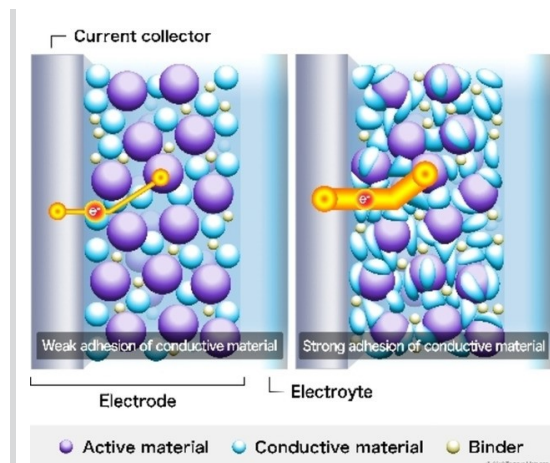
[< Previous Issue](#) | [Next Issue >](#) **GO TO SECTION****» Export Citation(s)****Cover Pictures** [Free Access](#)**Cover Picture: (21/2020)**

Pages: 6236 | First Published: 02 June 2020

[Abstract](#) | [Full text](#) | [PDF](#) | [Request permissions](#)**Communications****Electro, Physical & Theoretical Chemistry****Reversible Electrochemical Reaction of a Fluoride Shuttle Battery with a Bismuth(III) Fluoride Electrode and Electrolyte Containing Triphenylboroxine as an Anion Acceptor**

Dr. Hiroaki Konishi, Prof. Taketoshi Minato, Prof. Takeshi Abe, Prof. Zempachi Ogumi

Pages: 6237-6241 | First Published: 02 June 2020



Electrochemical reaction of fluoride shuttle battery with a BiF_3 electrode was evaluated in an electrolyte composed of G4, CsF, and TPhBX. The reversible capacity of an untreated BiF_3 electrode was low due to low electron conductivity of BiF_3 . Conversely, the reversible practical capacity of BiF_3 electrode was greatly improved by its stronger adhesion to conductive material.

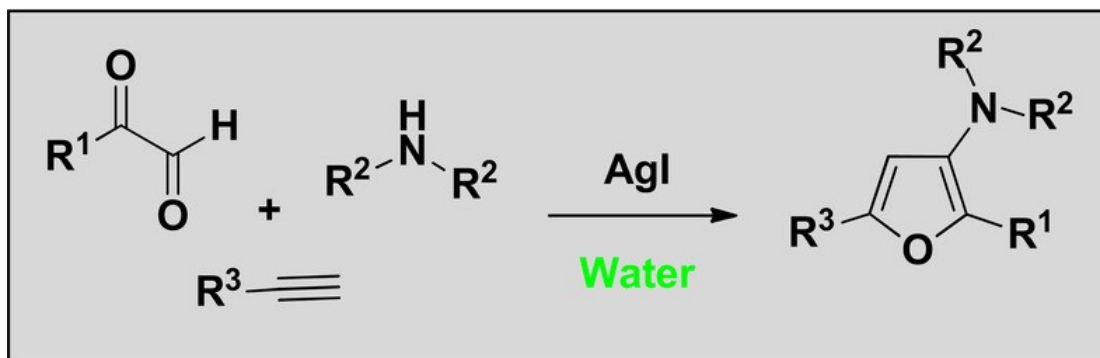
[Abstract](#) | [Full text](#) | [PDF](#) | [References](#) | [Request permissions](#)

Catalysis

Silver-Iodide-Catalyzed One-Pot Three-Component Synthesis of 3-Amino Furans in Water

Siva Kumar Rapeti, Krishna Chaitanya Kasina, Dr. Prasad Gundepaka, Dr. Saritha Birudaraju, Dr. Sailaja B. B. V

Pages: 6242-6244 | First Published: 02 June 2020



We herein, first time reported the easily accessible as well as inexpensive silver iodide promoted one-pot three-component reaction of 2-ketoaldehydes, secondary amines and terminal alkynes for the synthesis of 3-amino furans in moderate to high yields in environmentally benign water medium that proceeds through the tandem Mannich-Grignard addition followed by intramolecular cyclization. In addition, the efforts are under growth for the expansion of substrate scope.

[Abstract](#) | [Full text](#) | [PDF](#) | [References](#) | [Request permissions](#)

Full Papers

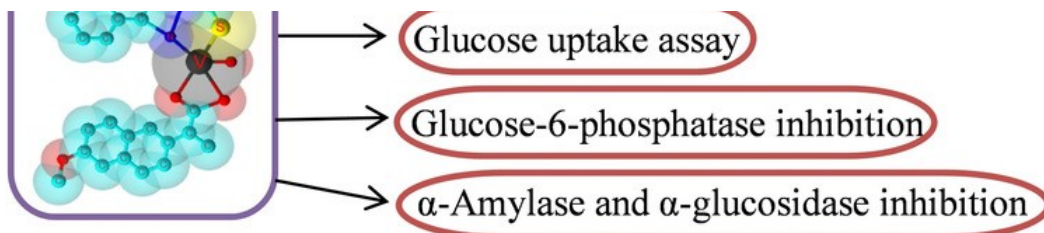
Materials Science inc. Nanomaterials & Polymers

In Vitro Antioxidant and Insulin Mimetic Activities of Heteroleptic Oxovanadium(IV) Complexes with Thiosemicarbazones and Naproxen

Sundaram Bharathi, Dr. Dharmasivam Mahendiran, Prof. Raju Senthil Kumar, Dr. Aziz Kalilur Rahiman

Pages: 6245-6254 | First Published: 02 June 2020





A series of heteroleptic oxovanadium(IV) complexes containing thiosemicarbazones as the main ligand and naproxen as auxiliary ligand with general formula $[\text{VOL}^{1-6}(\text{nap})]$ (**1–6**), where $\text{L}^{1-3} = 2-(1-(4\text{-substitutedphenyl})\text{ethylidene})\text{hydrazinecarbothio-amide}$, $\text{L}^{4-6} = 2-(1-(4\text{-substitutedphenyl})\text{ethylidene})\text{-N-methylhydrazinecarbothioamide}$ and $\text{nap} = \text{naproxen}$ were synthesized, which showed non-cytotoxic nature towards 3T3-L1 adipocyte cells and higher glucose uptake ability. In vitro inhibition against glucose-6-phosphatase, α -amylase and α -glucosidase enzymes showed better activity compared to the standard drugs, acarbose and metformin.

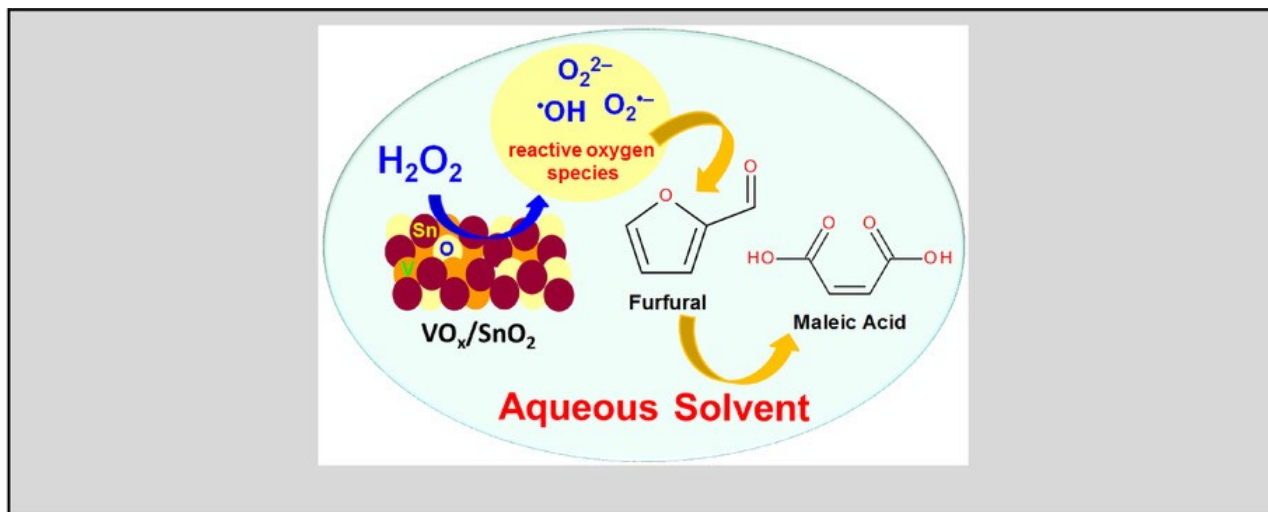
[Abstract](#) | [Full text](#) | [PDF](#) | [References](#) | [Request permissions](#)

Catalysis

Heterostructured Redox-Active $\text{V}_2\text{O}_5/\text{SnO}_2$ Oxide Nanocatalyst for Aqueous-Phase Oxidation of Furfural to Renewable Maleic Acid

Petrus M. Malibo, Prof. Peter R. Makgwane, Prof. Priscilla G. Baker

Pages: 6255-6267 | First Published: 02 June 2020



Nanostructuring vanadium and tin into hetero-mixed metal oxide interface (VO_x/SnO_2) provide an effect redox-active catalysts for mild oxidation of furfural to renewable maleic acid. At low V-metal loadings the catalyst is populated with the presence of VO_x monomeric and polymeric species which induce a highly active sites arising from the concomitant contribution from $\text{V}^{5+}/\text{V}^{4+}$ redox coupled to acidic sites of SnO_2 oxide.

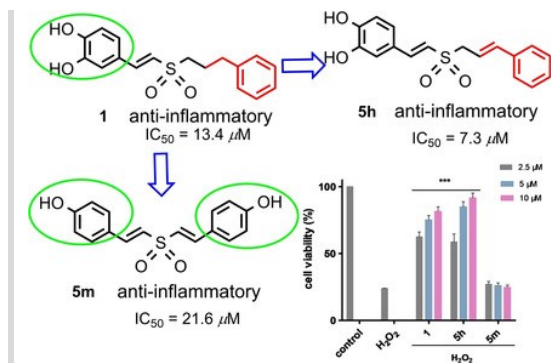
[Abstract](#) | [Full text](#) | [PDF](#) | [References](#) | [Request permissions](#)

Biological Chemistry & Chemical Biology

Design, Synthesis and Biological Evaluation of Novel (*E*)-Hydroxystyryl Aralkyl Sulfones as Neuroprotective Agents

Dr. Ying Chen, Yameng Hao, Qian Liu, Bolin Wu, Yunqi Liu, Prof. Zhili Zhang, Dr. Chao Tian, Dr. Xianling Ning, Dr. Ying Guo, Prof. Xiaowei Wang, Prof. Junyi Liu

Pages: 6268-6273 | First Published: 02 June 2020



In this paper, we focus on the role of catechol and phenyl in antioxidant and anti-inflammatory activities. We find that catechol group is essential for the antioxidant activity, but not that important for anti-inflammatory property. In addition, more than two phenolic hydroxyl groups reduced neuroprotective effects may be due to low permeability through cell membrane. Cinnamyl substituted phenylpropyl enhances the compound's anti-inflammatory activity.

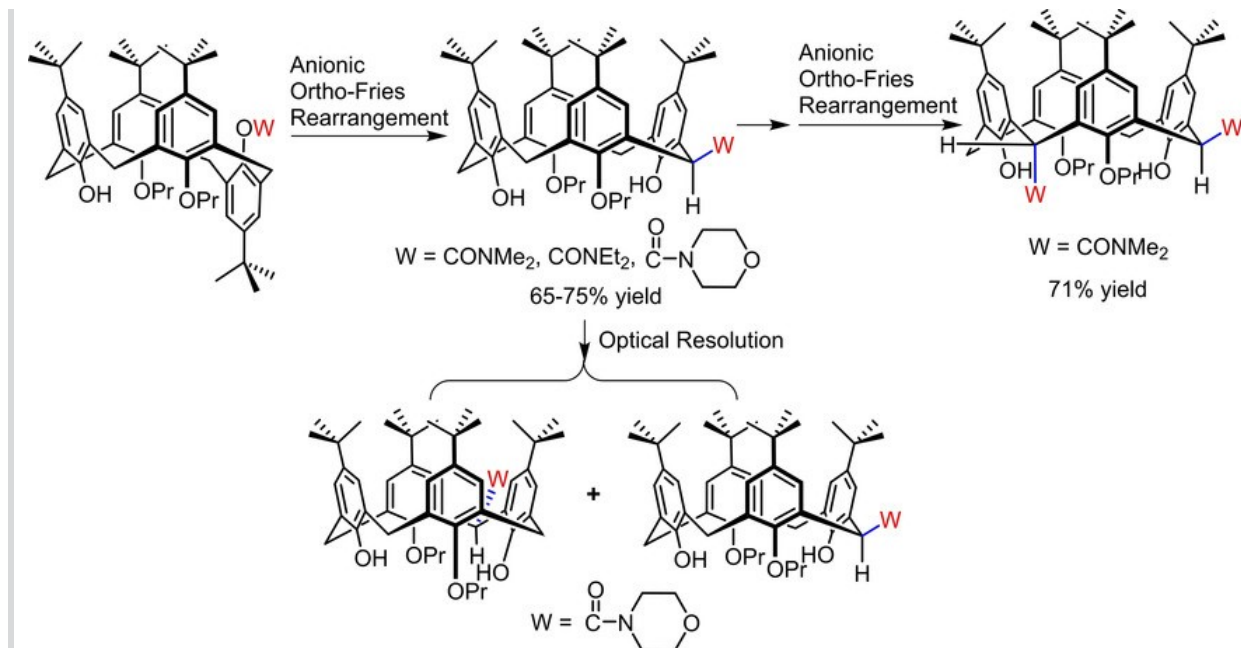
[Abstract](#) | [Full text](#) | [PDF](#) | [References](#) | [Request permissions](#)

Organic & Supramolecular Chemistry

Synthesis of Bridging Chiral *p*-*tert*-Butylcalix[4]arenes with One and Two Carbamoyl Bridge-Substituents through Anionic Ortho-Fries Rearrangement

Hao Ma, Xiu-Fang Weng, Shan-Shan Ren, Zi-Ying Tang, Xin-Bang Peng, Yong He, Shuang Zheng, Prof. Wei-Li Dong, Prof. Shao-Yong Li

Pages: 6274-6277 | First Published: 02 June 2020



Bridging chiral *p*-*tert*-butylcalix[4]arenes (BCC's) with different *N*-substituted carbamoyl bridge-substituents (*N,N*-dimethylcarbamoyl, *N,N*-diethylcarbamoyl and morpholinocarbonyl) from mono-*O*-carbamates of 1,3-dipropyl-*p*-*tert*-butylcalix[4]arene in 65–75% yield. In addition, *p*-*t*-Bu-BCC with two *N,N*-dimethylcarbamoyl bridge-substituents was prepared from mono-*O*-carbamate of *p*-*t*-Bu-BCC with one *N,N*-dimethylcarbamoyl bridge-substituent by this method in 71% yield. Finally, the racemic *p*-*t*-Bu-BCC with morpholinocarbonyl bridge-substituent was optically resolved into a pair of enantiomers.

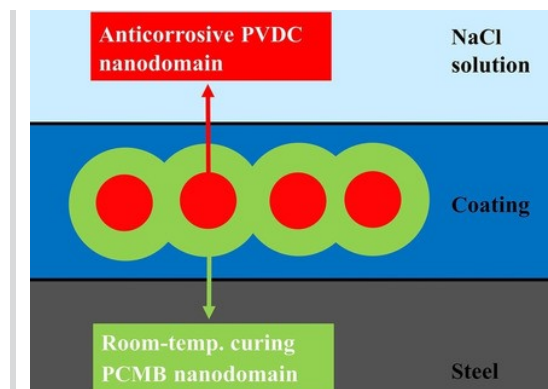
[Abstract](#) | [Full text](#) | [PDF](#) | [References](#) | [Request permissions](#)

Materials Science inc. Nanomaterials & Polymers

Poly(vinylidene chloride)/Poly(chlorotrifluoroethylene-co-acrylates) Composite Latex Coating Cured at Room Temperature Showing an Excellent Corrosion Resistance

Yanxu Wang, Chao Li, Xiaopeng Zhang, Qianqian Lin, Yuan Jiang, Prof. Jinfeng Yuan, Prof. Mingwang Pan

Pages: 6278-6284 | First Published: 02 June 2020



Poly(vinylidene chloride)/poly(chlorotrifluoroethylene-co-acrylates) (PVDC/PCMB) core-shell latex particles were prepared via seeded emulsion copolymerization of PVDC seeds with chlorotrifluoroethylene (CTFE), methyl methacrylate (MMA), and butyl acrylate (BA) comonomers. By the synergistic effect of PCMB and PVDC nanodomains, PVDC/PCMB latex particles can easily form a composite coating at room temperature, which can protect steel well for more than 400 h when immersed in 3.5 wt % NaCl solution. Therefore, PVDC/PCMB waterborne coating will have a potential application for heavy duty anticorrosion.

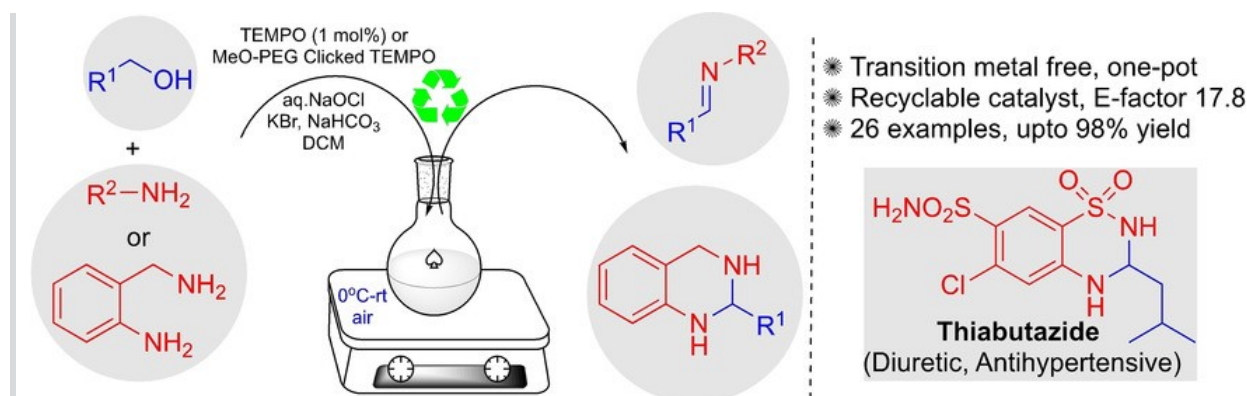
[Abstract](#) | [Full text](#) | [PDF](#) | [References](#) | [Request permissions](#)

Catalysis

Oxidative Cross-Coupling of Alcohols and Amines Catalyzed by TEMPO under Transition-Metal-Free Condition

Revathi Chandrasekaran, Elgin Carlose, Ajun E. Muthu, Athira Suresh, Dr. Tamilselvi Chinnusamy

Pages: 6285-6293 | First Published: 02 June 2020



A general and practical one-pot method for the synthesis of imines and 1,2,3,4-tetrahydroquinazolines was reported using 2,2,6,6-tetramethylpiperidine-1-oxyl (TEMPO) in combination with eco-friendly co-oxidant aq. NaOCl under transition-metal-free condition. The oxidative cross-coupling reaction also carried out using recyclable catalyst, afforded good yields of desired products. This method has successfully utilized to the synthesis of biologically important thiabutazide molecule in gram scale directly from alcohol and amine.

[Abstract](#) | [Full text](#) | [PDF](#) | [References](#) | [Request permissions](#)

Organic & Supramolecular Chemistry

Synthesis of Cinchona Urea Polymers and Their Evaluation as Catalyst in the Asymmetric Reactions

Mahmoud A. Abdelkawy, Prof. El-Saied A. Aly, Prof. Mahmoud A. El-Badawi, Prof. Shinichi Itsuno

Pages: 6294-6298 | First Published: 02 June 2020

Cinchona alkaloid polyurea catalyst: Mizoroki-Heck polymerization of cinchona urea dimer and 1,4-diiodobenzene gave a new type of chiral polyurea, which showed excellent catalytic activity in asymmetric Michael reactions. Up to >99% ee of the product was obtained with the polyurea catalyst which can be reused several times without any loss of the activity.

[Abstract](#) | [Full text](#) | [PDF](#) | [References](#) | [Request permissions](#)

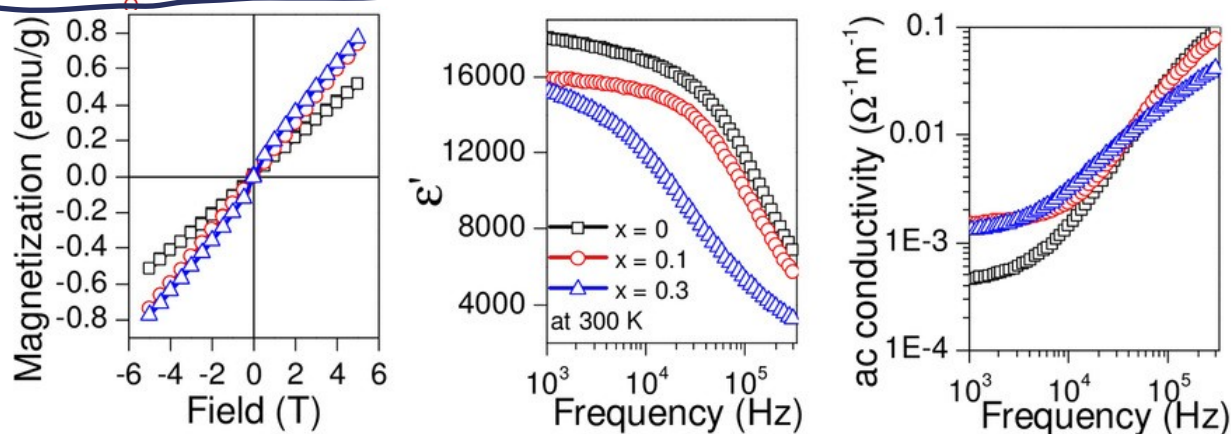
Materials Science inc. Nanomaterials & Polymers

Synthesis of $\text{Sr}_{1+x}\text{La}_{1-2x}\text{Fe}_{1-x}\text{Nb}_x\text{O}_4$ ($x=0, 0.1, 0.3$ and 0.5) by Sol-gel Method: Structural, Magnetic, and Dielectric Properties

Arif Kurnia, Prof. Entriadi, Dr. Nandang Mufti, Dr. Zulhadjri

Polyurea catalyst

Pages: 6299-6304 | First Published: 02 June 2020



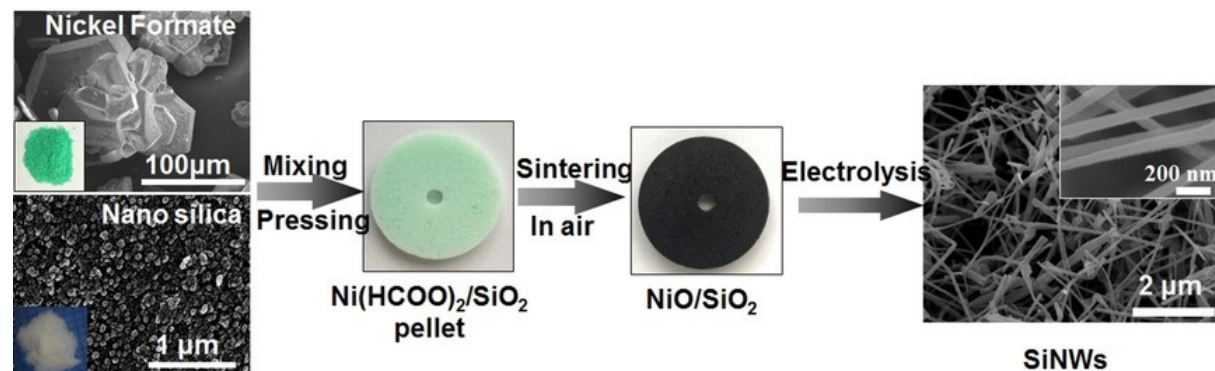
The new Ruddlesden-Popper $\text{Sr}_{1+2x}\text{La}_{1-2x}\text{Fe}_{1-x}\text{Nb}_x\text{O}_4$ with $x=0, 0.1$ and 0.3 was prepared successfully by sol-gel method. It can be seen that the magnetization and conductivity value increased with x increased, while dielectric constant decreased.

[Abstract](#) | [Full text](#) | [PDF](#) | [References](#) | [Request permissions](#)

In Situ Formation of Nickel Nanoparticles from Nickel Formate for Preparation of Straight Silicon Nanowires by Molten Salt Electrolysis

Dr. Zhanglong Yu, Dr. Sheng Fang, Jie Zhang, Bimeng Shi, Zhixia Shi, Prof. Juanyu Yang

Pages: 6305-6311 | First Published: 02 June 2020



Smooth and straight silicon nanowires (SiNWs) were prepared with nickel formate as the catalyst precursor by molten salt electrolysis of silica. The changes of Ni and NiO particles, which were obtained by decomposing nickel formate in N_2 and air, respectively, were disclosed during the silica reduction process. The obtained SiNWs exhibited excellent performance as the negative electrode material for lithium ion batteries.

[Abstract](#) | [Full text](#) | [PDF](#) | [References](#) | [Request permissions](#)

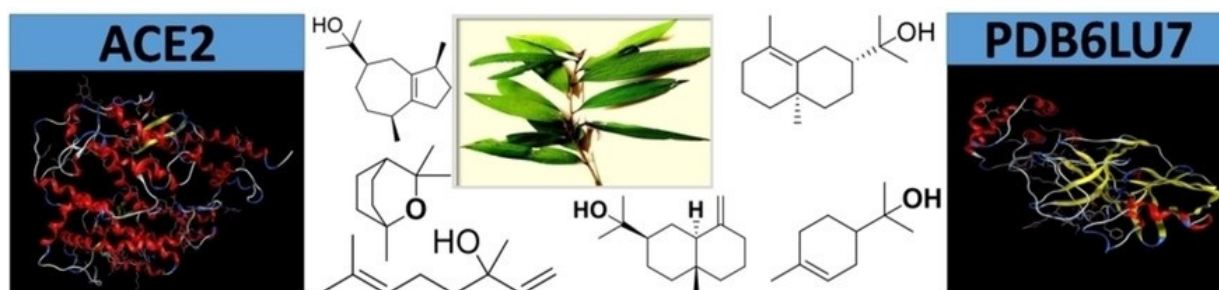
Biological Chemistry & Chemical Biology

[Free Access](#)

Evaluation of the Inhibitory Activities of COVID-19 of *Melaleuca cajuputi* Oil Using Docking Simulation

Dr. Tran Thi Ai My, Huynh Thi Phuong Loan, Nguyen Thi Thanh Hai, Dr. Le Trung Hieu, Prof. Tran Thai Hoa, Dr. Bui Thi Phuong Thuy, Prof. Duong Tuan Quang, Dr. Nguyen Thanh Triet, Dr. Tran Thi Van Anh, Dr. Nguyen Thi Xuan Dieu, Dr. Nguyen Tien Trung, Dr. Nguyen Van Hue, Dr. Pham Van Tat, Dr. Vo Thanh Tung, Dr. Nguyen Thi Ai Nhung

Pages: 6312-6320 | First Published: 02 June 2020



This is the first time to simulate the inhibitory effect of compounds in *Melaleuca cajuputi* oil to the main proteins of SARS-CoV-2 (PDB6LU7) and its host receptor (ACE2). They are strongly inhibited by the individual inhibition as well as the synergistic interaction of 10 out of 24 compounds accounting for 70.9% in this oil. The results orient that *Melaleuca cajuputi* oil is considered as a valuable resource for SARS-CoV-2 prevention.

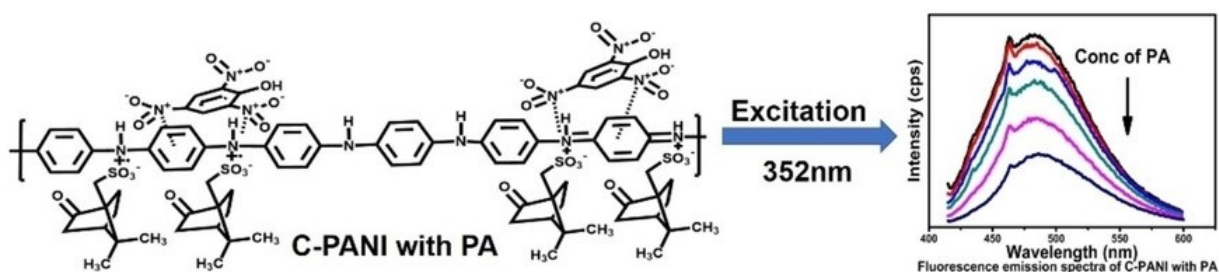
[Abstract](#) | [Full text](#) | [PDF](#) | [References](#) | [Request permissions](#)

Materials Science inc. Nanomaterials & Polymers

Mechanistic Insight into the Turn-Off Sensing of Nitroaromatic Compounds Employing Functionalized Polyaniline

Dr. Lakshmidevi Venkatappa, Satish Ashok Ture, Dr. Channabasaveshwar V. Yelamagad, Prof. Venkata Narayanan Naranammalpuram Sundaram, Prof. Ramón Martínez-Máñez, Prof. Venkataraman Abbaraju

Pages: 6321-6330 | First Published: 04 June 2020



A Functionalized polyaniline (C-PANI) as fluorophore is employed for sensing of Picric acid (PA) and p-nitro toluene (pNT) analytes in trace levels through fluorescence turn off mechanism with good sensitivity. The quenching mechanism involves photoinduced electron transfer. The bipolaronic and polaronic group interaction between C-PANI and analyte is studied by FTIR and Resonance Raman spectra for understanding mechanism of interaction. Further fluorescence studies are collaborated with electrochemical approach employing cyclic voltameter.

[Abstract](#) | [Full text](#) | [PDF](#) | [References](#) | [Request permissions](#)

Inorganic Chemistry

Role of Imidazole Co-Ligand in the Supramolecular Network of a Co(II) Complex with Sulfadiazine: Crystal Structure, Hirshfeld Surface Analysis and Energetic Calculations

Prof. Dr. Diego M. Gil, Prof. Dr. Hiram Pérez, Dr. Gustavo A. Echeverría, Dr. Oscar E. Piro, Prof. Dr. Antonio Frontera

Pages: 6331-6338 | First Published: 04 June 2020

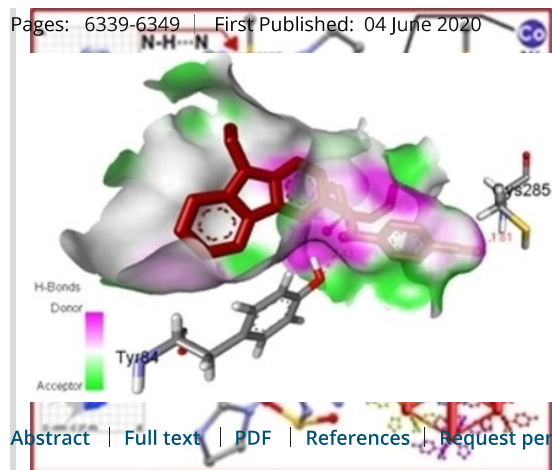
The role of imidazole co-ligand in the supramolecular network of a Co(II) complex in a new series of complexes with sulfadiazine is studied using several tools: X-ray diffraction, Hirshfeld surface analysis and energetic calculations.

[Abstract](#) | [Full text](#) | [PDF](#) | [References](#) | [Request permissions](#)

Organic & Supramolecular Chemistry

Green Synthesis Using PEG-400 Catalyst, Antimicrobial Activities, Cytotoxicity and In Silico Molecular Docking of New Carbazole Based on α -Aminophosphonate

Dr. Tran Nguyen Minh An, Prof. Nguyen Van Cuong, Dr. Nguyen Minh Quang, Prof. Truong Vu Thanh, Dr. Mahboob Alam



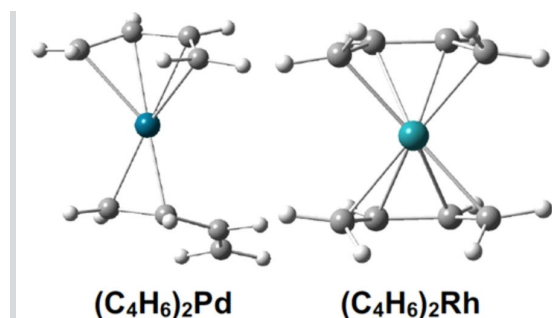
A new cytotoxicity compound **3f** elucidated the equivalent result *in vitro* ($IC_{50} = 5.16 \pm 0.04 \mu M$) and calculated a docking pose ($K_i = 0.039 \mu M$ and $\Delta G = -10.11 \text{ kcal.mol}^{-1}$) among the high inhibition compounds against HeLa, cervical cancer cell lines (PDB: 5HES). The most stable conformation **3f** formed two hydrogen bonds with the active sites of the receptor, 5HES (B:Cys285:N- **3f**: N, the bond length of 1.81 Å, and **3f**: H-A:Tyr84:O, 2.43 Å).

Inorganic Chemistry

Increasing the Ligand Field Strength in Butadiene Open Sandwich Compounds from the First to the Second Row Transition Metals

Dr. Junfeng Qian, Prof. Qun Chen, Prof. Mingyang He, Prof. Zhihui Zhang, Prof. Xuejun Feng, Dr. Yaoming Xie, Prof. R. Bruce King, Prof. Henry F. Schaefer

Pages: 6350-6359 | First Published: 04 June 2020



The second-row transition metals energetically prefer low spin states in their bis(butadiene) derivatives $(C_4H_6)_2M$ reflecting their increased ligand field strength relative to the first-row transition metals. Staggered maximum spin $(C_4H_6)_2M$ structures having tetrahedral coordination of the central metal to the four C=C double bonds of the two butadiene ligands are not found.

Abstract | Full text | PDF | References | Request permissions

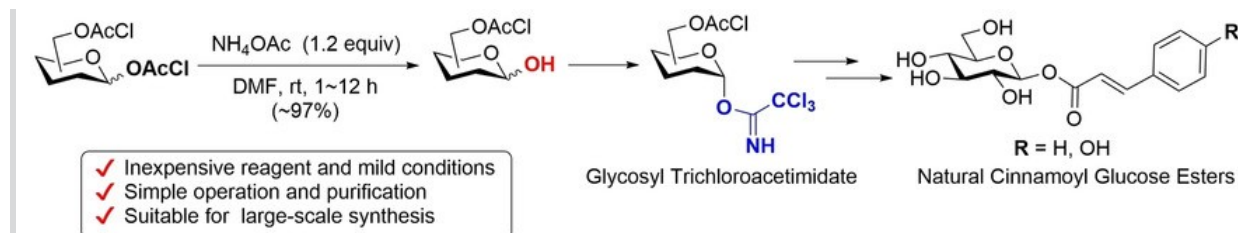
Communications

Organic & Supramolecular Chemistry

Regioselective Dechloroacetylations Mediated by Ammonium Acetate: Practical Syntheses of 2,3,4,6-Tetra-O-chloroacetyl-glycopyranoses and Cinnamoyl Glucose Esters

Dr. Penghua Shu, Haoying Niu, Lingxiang Zhang, Haichang Xu, Mengzhu Yu, Junping Li, Xue Yang, Yingying Fei, Hao Liu, Dr. Zhiyu Ju, Prof. Zhihong Xu

Pages: 6360-6364 | First Published: 24 June 2020



2,3,4,6-Tetra-O-chloroacetyl-glycopyranoses: An ammonium acetate (NH_4OAc)-mediated regioselective dechloroacetylations in carbohydrates is developed, which enables the efficient large-scale synthesis of 2,3,4,6-tetra-O-chloroacetyl-glycopyranoses under mild reaction conditions.

The synthetic value of this protocol is further illustrated in the preparation of two natural cinnamoyl glucose esters.

[Abstract](#) | [Full text](#) | [PDF](#) | [References](#) | [Request permissions](#)

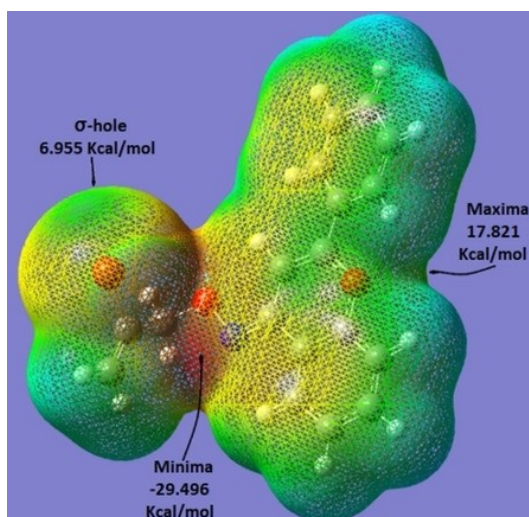
Full Papers

Organic & Supramolecular Chemistry

Spectroscopic (FTIR and UV-Vis) Analysis, Supramolecular Studies, XRD Structural Characterization and Theoretical Studies of Two Flavone-Oxime Derivatives

Prof. Rodolfo Moreno-Fuquen, Vanessa Morales, Dr. Alix Loaiza, Dr. Juan Carlos Tenorio, Prof. Richard Goddard

Pages: 6365-6372 | First Published: 04 June 2020



Two flavone-oxime derivatives were analyzed by single crystal XRD and UV-Vis and IR spectroscopy. Supramolecular studies revealed the existence of halogen C–Br...C_g bonds and C–H...O bonds. Quantitative MEP calculations showed the value over the σ -hole region. IR spectroscopy studies revealed the characteristic frequency values of N–O and N=C of these compounds. The analysis of the interaction energies between pairs of neighboring molecules showed that the dispersion term contributed essentially to the total interaction energy in the crystal formation.

[Abstract](#) | [Full text](#) | [PDF](#) | [References](#) | [Request permissions](#)

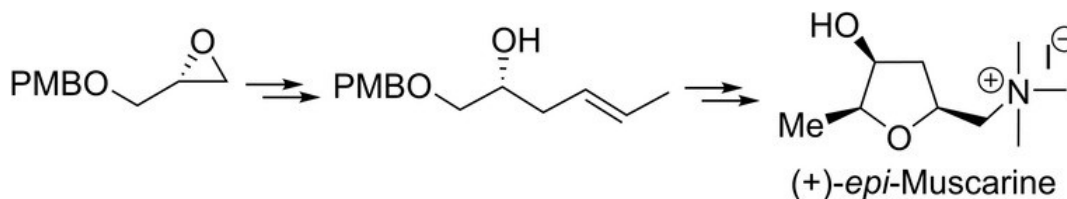
Communications

Organic & Supramolecular Chemistry

A Short and Efficient Enantioselective Synthesis of (+)-(2S,3S,5S)-*epi*-Muscarine

Anju Gehlawat, Prof. Ranjana Prakash, Dr. Satyendra Kumar Pandey

Pages: 6373-6375 | First Published: 05 June 2020



An efficient and novel general method for asymmetric synthesis of muscarine alkaloids and its application to the total synthesis of (+)-*epi*-muscarine from (*R*)-PMB glycidyl ether as starting material is presented. Key transformations include Sharpless asymmetric dihydroxylation (AD), regioselective epoxide ring opening and intramolecular S_N2 cyclization.

[Abstract](#) | [Full text](#) | [PDF](#) | [References](#) | [Request permissions](#)

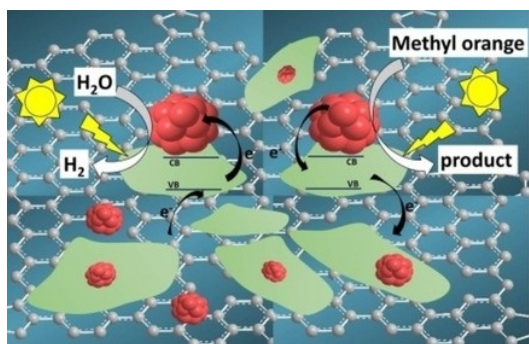
Full Papers

Catalysis

Photoelectrochemical Activity of Ag Coated 2D-TiO₂/RGO Heterojunction for Hydrogen Evolution Reaction and Environmental Remediation

Mohammad Saquib, Ravinder Kaushik, Aditi Halder

Pages: 6376-6388 | First Published: 22 June 2020



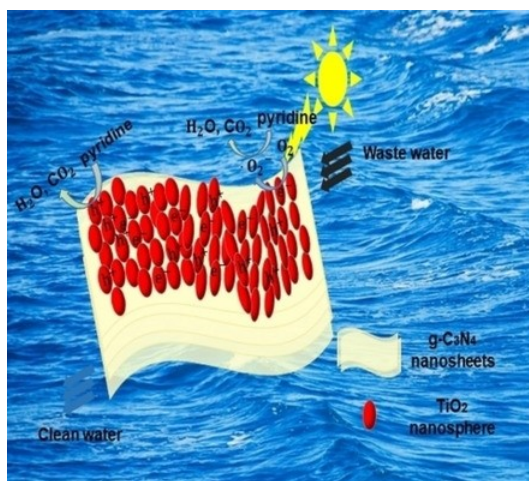
To demonstrate the plasmon effect of Ag NPs in Ag/TiO₂/RGO for HER and MO dyestuff degradation was studied. Ag/TiO₂/RGO performed better HER catalytic activity, stable and durable electrocatalyst. The photoelectrocatalytic HER activity of Ag/TiO₂/RGO showed that the photogenerated electrons and holes are driven away in opposite directions by Ag NPs and RGO and increases the photoelectrocatalytic H₂ generation from water. Ag/TiO₂/RGO showed the highest MO degradation silver NPs, delayed in the recombination rate of electron-hole pair of 2D-TiO₂ nanoflakes/ 2D rGO.

[Abstract](#) | [Full text](#) | [PDF](#) | [References](#) | [Request permissions](#)

Preparation and Kinetics of g-C₃N₄/TiO₂ Nanomaterials for the Photodegradation of Pyridine Under Solar-Light Irradiation

Min Liu, Xue Feng Tian, Dr. Yan Long Chang

Pages: 6389-6402 | First Published: 04 June 2020



In this work, g-C₃N₄/TiO₂ photocatalyst was successfully prepared, using low-temperature calcination. The photocatalytic performance of the catalyst was analyzed by various characterization methods, and it was used to photodegrade pyridine and other nitrogen heterocyclic organic solutions under visible light irradiation, the catalyst showed excellent photoactivity. As a highly active photocatalyst, it provides the feasibility for photocatalytic degradation of nitrogen heterocyclic organic solutions.

[Abstract](#) | [Full text](#) | [PDF](#) | [References](#) | [Request permissions](#)

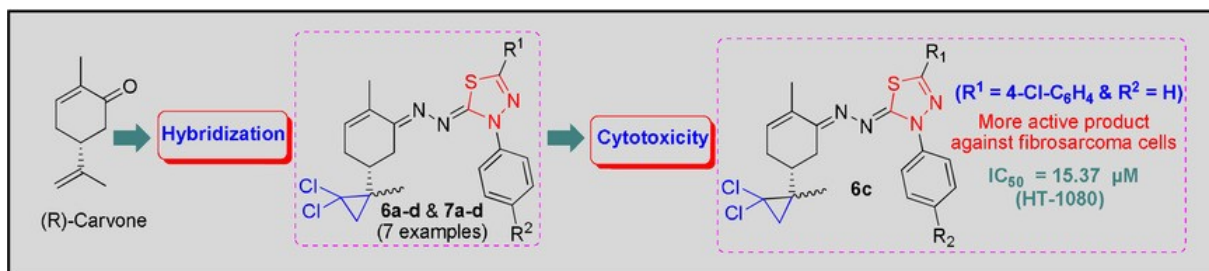
Communications

Medicinal Chemistry & Drug Discovery

Synthesis and Antitumor Activity of Novel Heterocyclic Systems with Monoterpenic Skeleton Combining Dichlorocyclopropane and 1,3,4-Thiadiazole Nucleus

Dr. Ali Oubella, Dr. Mourad Fawzi, Prof. Aziz Auhmani, Prof. Abdelkhalek Riahi, Prof. Hamid Morjani, Dr. Anthony Robert, Prof. Moulay Y. Ait Itto

Pages: 6403-6406 | First Published: 04 June 2020



An efficient and chemoselective three-step procedure was carried out from (R)-carvone to access new C(2)-N(4)-disubstituted 1,3,4-thiadiazoles paired with a dichlorocyclopropane core. These newly prepared dichlorocyclopropanic thiadiazoles have revealed interesting antitumor activity.

[Abstract](#) | [Full text](#) | [PDF](#) | [References](#) | [Request permissions](#)

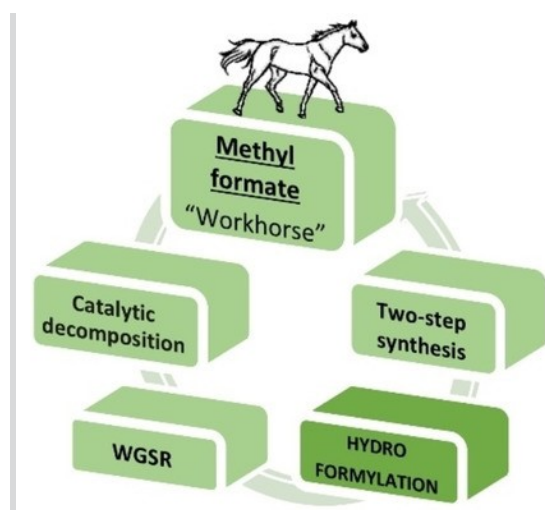
Full Papers

Sustainable Chemistry

Methyl Formate: How It Can Be Used as Formyl Group Source for Synthesis of Aldehydes via Hydroformylation?

Dr. Dmitry Gorbunov, Maria Nenasheva, Dr. Maria Terenina, Dr. Yulia Kardasheva, Prof. Anton Maksimov, Prof. Eduard Karakhanov

Pages: 6407-6414 | First Published: 04 June 2020



Methyl formate-water mixture was used as an alternative syngas source for hydroformylation and tandem hydroformylation-acetalization catalyzed by Rh/phosphine complexes. Aldehydes and cyclic acetals were the main products of olefin conversion. Various olefins were transformed into aldehydes by this method with sufficient yields. We suppose that byproducts of the reaction –CO₂, methanol, and hydrogen-may act as building blocks for further synthesis of methyl formate, providing an opportunity for its recirculation.

[Abstract](#) | [Full text](#) | [PDF](#) | [References](#) | [Request permissions](#)

Materials Science inc. Nanomaterials & Polymers

Comparative Insight into the Performance of Two Different Amine-Functionalized CNTs for the Chemical Speciation of Chromium

Dr. Niharika Sharma, Dr. Shelja Tiwari, Dr. Reena Saxena

Pages: 6415-6423 | First Published: 04 June 2020

This paper reports the performance comparison of two different amine functionalized nanoadsorbents for the preconcentrative speciation of chromium in a hyphenated FI-FAAS system. The prepared nanoadsorbents could selectively preconcentrate Cr(III) in the presence of Cr(VI) and other matrix components, thus leading to the speciation of Cr(III) from Cr(VI). The hyphenated system was applied to industrially contaminated water samples and >95 % recovery was achieved. The reported method is fast, selective, and highly reliable for chromium speciation in complex aqueous matrices.

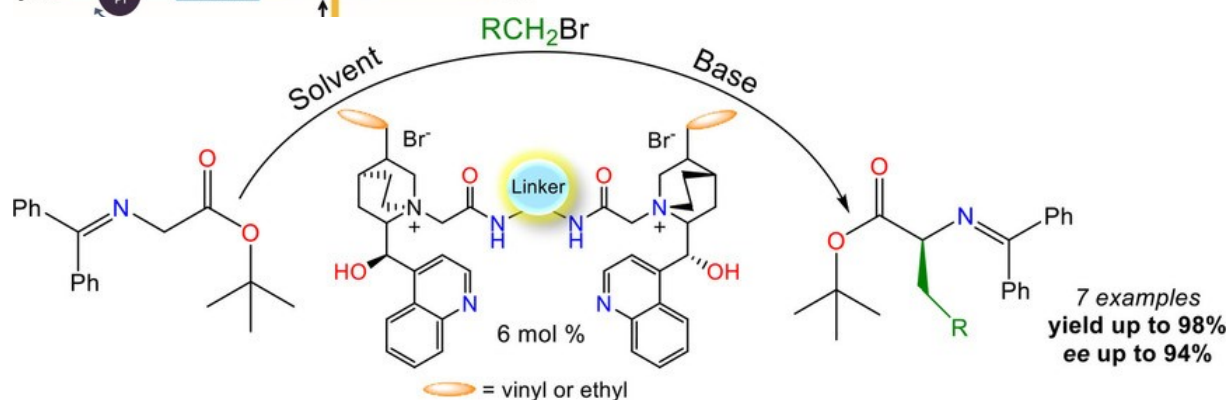
[Abstract](#) | [Full text](#) | [PDF](#) | [References](#) | [Request permissions](#)

Catalysis

Synthesis of C2 Hybrid Amide-Based PTC Catalysts and Their Comparison with Saturated Analogues

Dr. Maciej Majdecki, Dr. Patryk Niedziela, Prof. Janusz Jurczak

Pages: 642-649 | First Published: 04 June 2020



A novel family of *Cinchona* alkaloid C2 catalysts containing diamide linkers was designed. These hybrid derivatives were used in the asymmetric alkylation of glycine imine ester. Catalytic efficiency of the amide derivatives depends on the substituent in the phenyl ring. The corresponding alkylated products were obtained with excellent yields (up to 98%) and very high enantioselectivities (up to 94% ee) using various benzyl bromides. It was found that saturated catalysts exhibit higher selectivity in examined reaction.

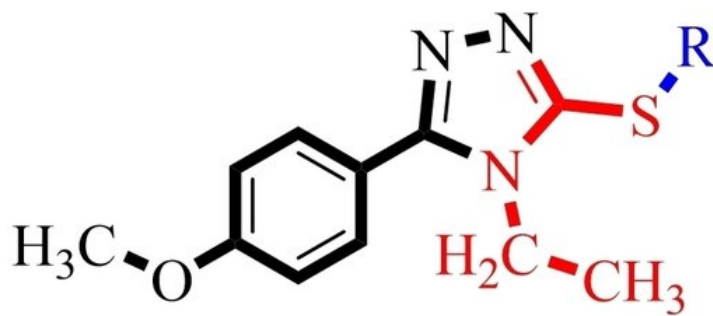
[Abstract](#) | [Full text](#) | [PDF](#) | [References](#) | [Request permissions](#)

Medicinal Chemistry & Drug Discovery

Discovery of Dual Inhibitors of Acetyl and Butyrylcholinesterase and Antiproliferative Activity of 1,2,4-Triazole-3-thiol: Synthesis and In Silico Molecular Study

Dr. Sabahat Zahra Siddiqui, Muhammad Arfan, Dr. Muhammad Athar Abbasi, Dr. Aziz-ur-Rehman, Dr. Syed Adnan Ali Shah, Dr. Muhammad Ashraf, Safdar Hussain, Rahman Shah Zaib Saleem, Rafaila Rafique, Prof. Dr. Khalid Mohammed Khan

Pages: 6430-6439 | First Published: 05 June 2020



S-Alkyl/Aralkylated 4-ethyl-5-(4-methoxyphenyl)-4H-1,2,4-triazole-3-thiols

S-Alkylated/arylated-4-ethyl-5-(4-methoxyphenyl)-4H-1,2,4-triazole-3-thiols were synthesized by multistep reaction. 4-Methoxybenzohydrazide and ethyl isothiocyanate were reacted in methanol to afford an intermediate *N*-ethyl-2-(4-methoxybenzoyl)hydrazinecarbothioamide which undergoes cyclization in aqueous alkaline media; 10% NaOH to yield 4-ethyl-5-(4-methoxyphenyl)-4H-1,2,4-triazole-3-thiol as parent compound which further react with alkylhalides in *N,N*-dimethylformamide in the presence of LiH as catalyst. Synthesized compounds were tested for their possible acetyl/butyrylcholinesterase enzymes inhibition.

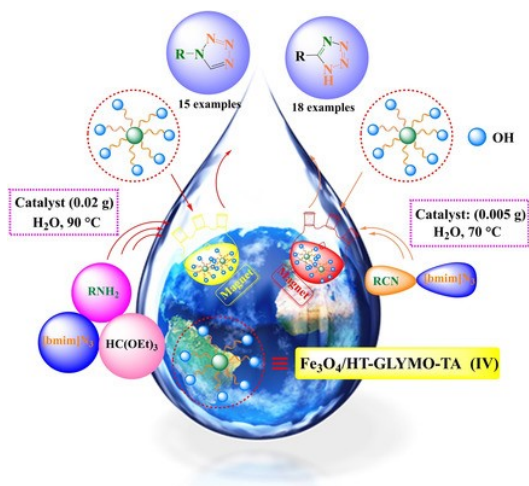
[Abstract](#) | [Full text](#) | [PDF](#) | [References](#) | [Request permissions](#)

Organic & Supramolecular Chemistry

An Eco-Friendly and Efficient Approach for the Synthesis of Tetrazoles *via* Fe₃O₄/HT-GLYMO-TA as a New Recoverable Heterogeneous Nanostructured Catalyst

Maryam Sadat Ghasemzadeh, Prof. Dr. Batool Akhlaghinia

Pages: 6440-6452 | First Published: 05 June 2020



In this research, tannic acid immobilized on functionalized magnetic hydrotalcite (Fe₃O₄/HT-GLYMO-TA (**IV**)) was prepared as a recyclable and efficient nanostructured catalyst for the syntheses of 5-substituted-1*H*- tetrazoles and 1-substituted-1*H*-1,2,3,4-tetrazoles in green media. The characterization of nanostructured catalyst showed that the new nanostructured catalyst has a plate-like shape, an average particle size of 23–27 nm and superparamagnetic behavior. The nanostructured catalyst can also be recycled at least eight times without a significant decrease in catalytic activity.

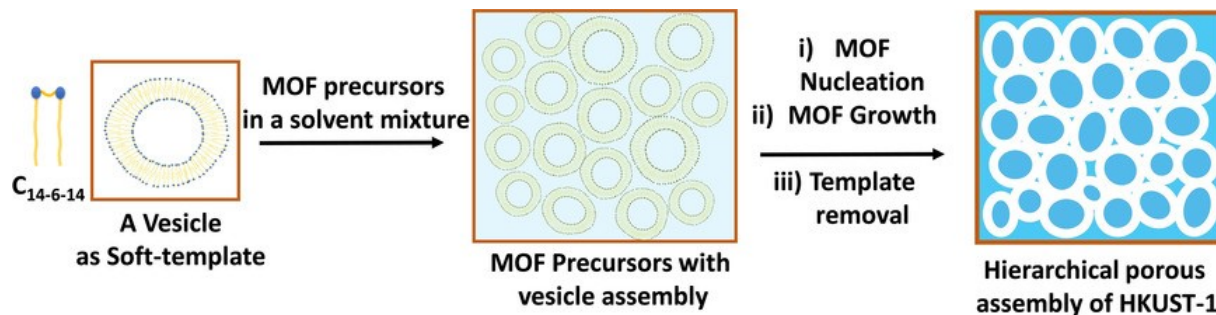
[Abstract](#) | [Full text](#) | [PDF](#) | [References](#) | [Request permissions](#)

Materials Science inc. Nanomaterials & Polymers

Synthesis of Hierarchically Porous HKUST-1 MOF: Use of C₁₄₋₆₋₁₄, a Cationic Gemini Surfactant, as Soft-Template †

Rajesh Ghosh, Dr. Thirumurugan Alagarsamy

Pages: 6453-6469 | First Published: 05 June 2020



Soft templated synthesis of hierarchically porous MOFs: Using a gemini surfactant, (C₁₄₋₆₋₁₄), in its vesicular assembled form as soft templates, hierarchically porous HKUST-1 MOF samples, with connected meso- and micropores have been prepared. Hierarchical factor (HF) is calculated to understand the varying degree of hierarchical porosity in the samples. The dye uptake in the prepared samples demonstrate the presence of mesopores in them and to correlate with the HFs.

[Abstract](#) | [Full text](#) | [PDF](#) | [References](#) | [Request permissions](#)

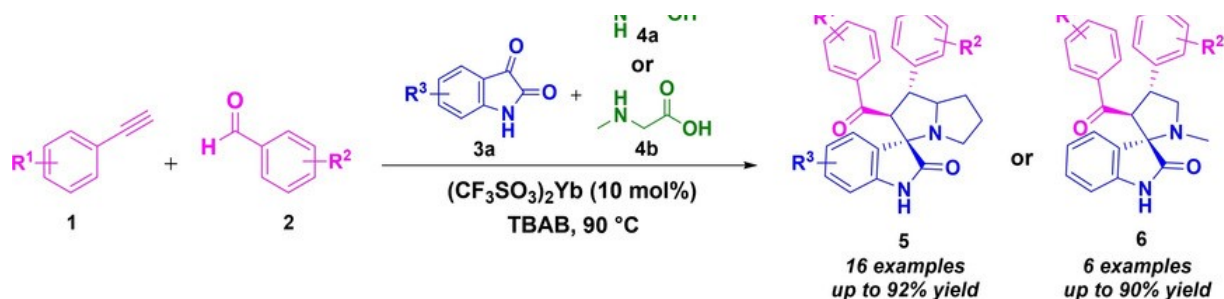
Organic & Supramolecular Chemistry

Tetrabutylammonium-Bromide-Promoted Synthesis of Spirooxindoles through Alkyne-Aldehyde C–C Coupling and 1,3-Dipolar Cycloaddition Using Ytterbium Triflate Catalyst

Chitrala Teja, Prof. Dr. Fazlur Rahman Nawaz Khan

Pages: 6470-6474 | First Published: 05 June 2020





A rare earth metal (Ytterbium triflate) catalyzed one-pot domino synthesis of spirooxindoles from hydration-condensation of alkyne, aldehyde, C–C coupling followed by 1,3-dipolar cycloaddition of azomethine ylide is described. Here, Tetrabutylammonium-bromide is used as efficient reaction medium; it is a green-chemical reaction medium to provide spirooxindoles in high regio and stereo selectivities and yields. Stereochemical outcomes of the synthesized molecules were characterized by 2D NMR Spectroscopic studies.

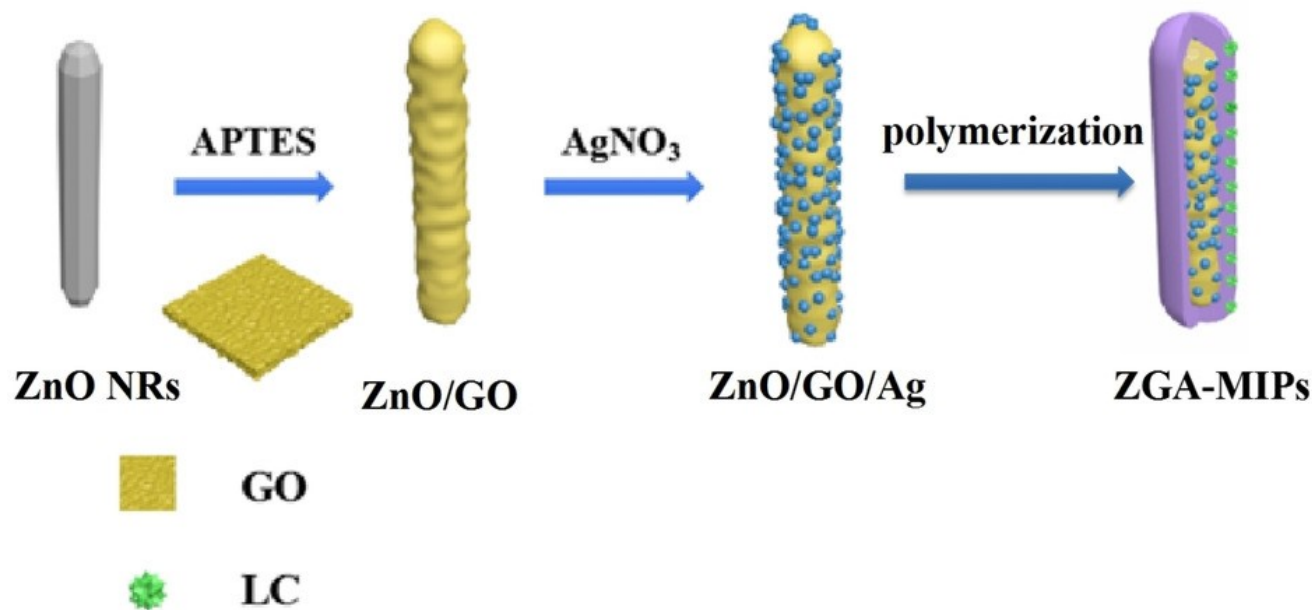
[Abstract](#) | [Full text](#) | [PDF](#) | [References](#) | [Request permissions](#)

Analytical Chemistry

Multifunction Sandwich Composite SERS Imprinted Sensor Based on ZnO/GO/Ag for Selective Detection of Cyfluthrin in River

Hongji Li, Chuqi Ren, Jingjing Meng, Yan Gao, Tong Ren, Yue Li, Yu Qiao, Chunbo Liu, Guangbo Che

Pages: 6475-6481 | First Published: 05 June 2020



In this manuscript, a novel sensor based on molecular imprinted polymers (MIPs) was synthesized. It was illustrated that the syntheses approach of ZGA-MIPs (ZnO/GO/Ag-MIPs). The ZGA-MIPs were synthesized by the procedure of precipitation polymerization. When the template molecules were rinsed, the specific recognition cavities could “freeze” on the surface of ZGA-MIPs. The ZGA-MIPs made contribution to selectively adsorbing and detecting template molecules. Furthermore, the ZGA-MIPs also presented the property of “self-cleaning” which could effectively degrade the contaminants on the surface.

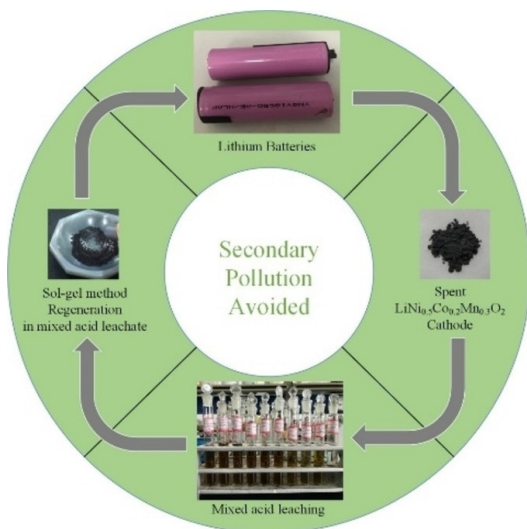
[Abstract](#) | [Full text](#) | [PDF](#) | [References](#) | [Request permissions](#)

Sustainable Chemistry

Recycling of LiNi_{0.5}Co_{0.2}Mn_{0.3}O₂ Material from Spent Lithium-ion Batteries Using Mixed Organic Acid Leaching and Sol-gel Method

Ruichuan Gao, Dr. Conghao Sun, Prof. Tao Zhou, Luqi Zhuang, Huasheng Xie

Pages: 6482-6490 | First Published: 05 June 2020



$\text{LiNi}_{0.5}\text{Co}_{0.2}\text{Mn}_{0.3}\text{O}_2$ cathode material of spent lithium batteries was leached out by organic mixed-acid. The mixed-acid leachate was used to regenerate fresh cathode material by sol-gel method. This process provides a novel and green recycling process of spent lithium batteries, and it has advantages of less reagents consumption and avoid secondary pollution.

[Abstract](#) | [Full text](#) | [PDF](#) | [References](#) | [Request permissions](#)

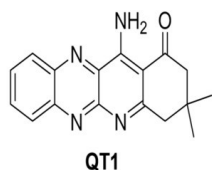
Communications

Organic & Supramolecular Chemistry

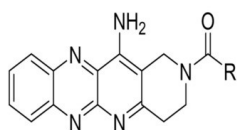
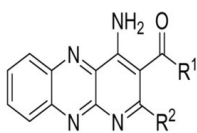
Automated Synthesis of New Quinoxalinetacrine

Dr. Óscar M. Bautista-Aguilera, Prof. Lhassane Ismaili, Dr. Mourad Chioua, Prof. Isabel Iriepa, Dr. María Ángeles Martínez-Grau, Christopher D. Beadle, Tatiana Vetman, Prof. Francisco López-Muñoz, Prof. José Marco-Contelles

Pages: 6491-6493 | First Published: 05 June 2020



QuinoxalineTacrines QT1-11, designed by juxtaposition of tacrine and quinoxaline, have been obtained from 3-aminoquinoxaline-2-carbonitrile and suitable commercially available ketones, by Lewis-acid catalyzed Friedländer reaction.


[Abstract](#) | [Full text](#) | [PDF](#) | [References](#) | [Request permissions](#)

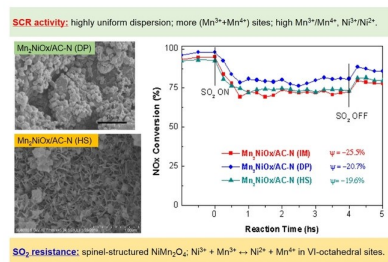
Full Papers

Catalysis

Novel Ni-Mn Bi-oxides Doped Active Coke Catalysts for NH₃-SCR De-NO_x at Low Temperature

Chengzhi Wang, Zaharaddeen Sani, Prof. Xiaolong Tang, Yuhe Wang, Prof. Honghong Yi, Prof. Fengyu Gao

Pages: 6494-6503 | First Published: 05 June 2020



Spinel-structured NiMn₂O₄ might be one important reason for high activity and SO₂-resistance. Good SCR activity might be attributed to more (Mn³⁺+Mn⁴⁺), high Mn³⁺/Mn⁴⁺ and Ni³⁺/Ni²⁺. Probable [Ni²⁺Mn⁴⁺]_{tet}[Ni²⁺Ni³⁺Mn³⁺Mn⁴⁺]_{oct}O₄ configconstruct benefits for electronic transfers (Ni³⁺+Mn³⁺ ↔ Ni²⁺+Mn⁴⁺) in VI-octahedral sites.

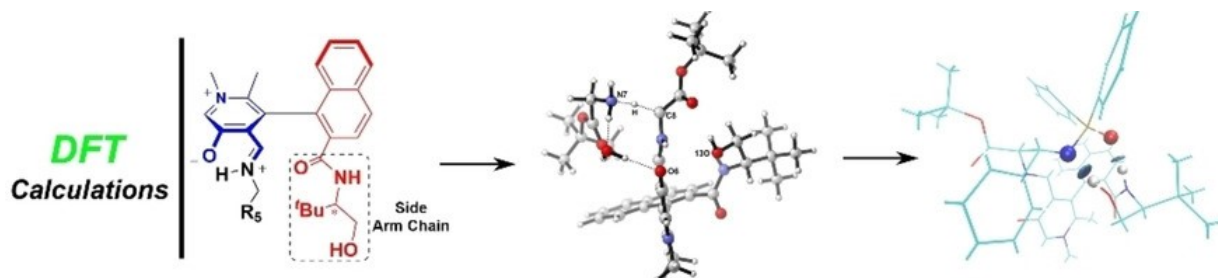
[Abstract](#) | [Full text](#) | [PDF](#) | [References](#) | [Request permissions](#)

Electro, Physical & Theoretical Chemistry

Computational Insight into the Mechanism of Mannich Reaction between Glycinate and Aryl *N*-Diphenylphosphinyl Imine Catalyzed by *N*-Quaternized Pyridoxal

Dr. Yongsheng Yang, Dr. Yan Zhang, Junxia Yang, Prof. Ying Xue

Pages: 6504-6513 | First Published: 05 June 2020



The pyridoxal-catalyzed Mannich reaction between *tert*-butyl glycinate and aryl *N*-diphenylphosphinyl imine, was studied by Density Functional Theory (DFT) method. The specific deprotonation processes were figured out to achieve α -carbon deprotonation which is activated by pyridoxal catalyst. Phenolic oxyanion, *tert*-butyl glycinate, and OH⁻ can act as catalytic base. During addition reaction for C–C bond formation, *N*-diphenylphosphinyl imine establishes strong hydrogen-bonding interaction with side arm chain of pyridoxal catalyst.

[Abstract](#) | [Full text](#) | [PDF](#) | [References](#) | [Request permissions](#)

Catalysis


Graphene Oxide Catalyzed One-pot Synthesis of Pyrimido[4,5-*b*]quinolinone-2,4-diones and their Biological Evaluation

Rabindranath Singha, Puja Basak, Malay Bhattacharya, Pranab Ghosh

Pages: 6514-6525 | First Published: 05 June 2020

An environmentally benign three component synthesis of pyrimido[4,5-*b*]quinolinone-2,4-diones using GO as novel carbocatalyst has been described. GO was proved to be a highly efficient catalyst for this one pot synthesis and reused upto 5th run without losing its catalytic activity. Antimicrobial activity of some of the synthesized pyrimido[4,5-*b*]quinolinone-2,4-diones were also carried out to establish the importance of this promising heterocyclic moiety.

[Abstract](#) | [Full text](#) | [PDF](#) | [References](#) | [Request permissions](#)

 [Submit a Manuscript](#)
 [Browse free sample issue](#)
 [Get content alerts](#)
 [Subscribe to this journal](#)



$R = -CH_3, -OCH_3, -NO_2, -Cl, -F, -OH$
 $R_1 = -CH_3, -Cl, -Br$

More from this journal

[Reviews](#)
[Editorials](#)
[Video Abstracts](#)

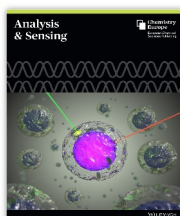
One App
18 chemical society journals



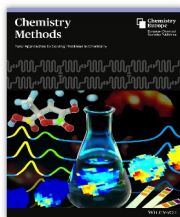




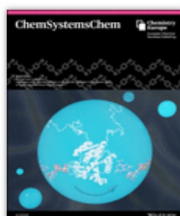

Chemistry Europe
 European Chemical Societies Publishing



NEW JOURNAL:
[Analysis & Sensing](#)
 Accepting submissions now.



NEW JOURNAL:
[Chemistry—Methods](#)
 Accepting submissions now.



ISSUE
 Volume 2, Issue 4
 July 2020



ISSUE

Volume 26, Issue 43

Pages: 9403-9651

August 3, 2020

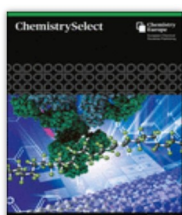


ISSUE

Volume 9, Issue 8

Pages: 793-817

August 2020

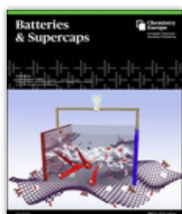


ISSUE

Volume 5, Issue 29

Pages: 8881

August 7, 2020

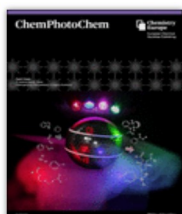


ISSUE

Volume 3, Issue 7

Pages: 566-667

July 2020

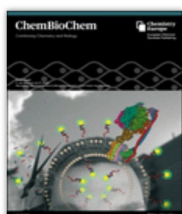


ISSUE

Volume 4, Issue 7

Pages: 451-534

July 2020



ISSUE

Volume 21, Issue 15

Pages: 2086-2224

August 3, 2020

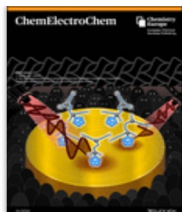


ISSUE

Volume 12, Issue 14

Pages: 3598-3792

July 21, 2020

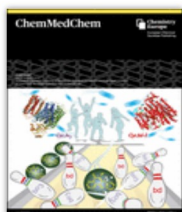


ISSUE

Volume 7, Issue 15

Pages: 3168-3310

August 3, 2020

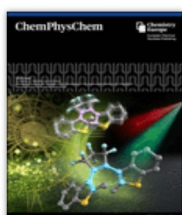


ISSUE

Volume 15, Issue 14

Pages: 1243-1371

July 20, 2020

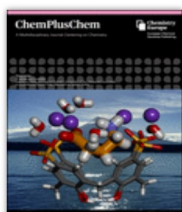


ISSUE

Volume 21, Issue 14

Pages: 1483-1616

July 17, 2020



ISSUE

Volume 85, Issue 8

Pages: 1612-1638

August 2020



ISSUE

Volume 13, Issue 14

Pages: 3539-3725

July 22, 2020



ISSUE

Volume 2020, Issue 29

Pages: 2767-2849

August 9, 2020



ISSUE

Volume 2020, Issue 29

Pages: 4433-4638

August 9, 2020



ChemistryViews.org Home

Your Chemistry Hero

03 Aug 2020

Who do you admire in chemistry? What makes a hero for you? – anniversary contest for August

Nanoparticle Catalyst with All Six Platinum-Group Metals

03 Aug 2020

High-entropy-alloy nanoparticles can catalyze complex reactions

Smelling Molecular Conformations

03 Aug 2020

Olfactory receptor recognizes different conformationally restricted octanal analogues

Chemistry Europe Virtual Events

02 Aug 2020

Virtual symposia and talks organized by the editorial offices and board members of Chemistry Europe journals

Electronics Waste Reused as Protective Coating

02 Aug 2020

Old printed circuit boards and computer monitors converted to strong coating for steel



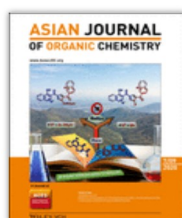
ISSUE

Volume 15, Issue 15

The Chemistry of 2D Materials Membranes

Pages: 2239-2378

August 3, 2020



ISSUE

Volume 9, Issue 7

Pages: 967-1086

July 2020



ISSUE

Volume 6, Issue 7

Pages: 996-1135

July 2020

© 2020 WILEY-VCH Verlag GmbH & Co. KGaA, Weinheim

[About Wiley Online Library](#)[Privacy Policy](#)[Terms of Use](#)[Cookies](#)[Accessibility](#)[Help & Support](#)[Contact Us](#)[Opportunities](#)[Subscription Agents](#)[Advertisers & Corporate Partners](#)[Connect with Wiley](#)[The Wiley Network](#)[Wiley Press Room](#)

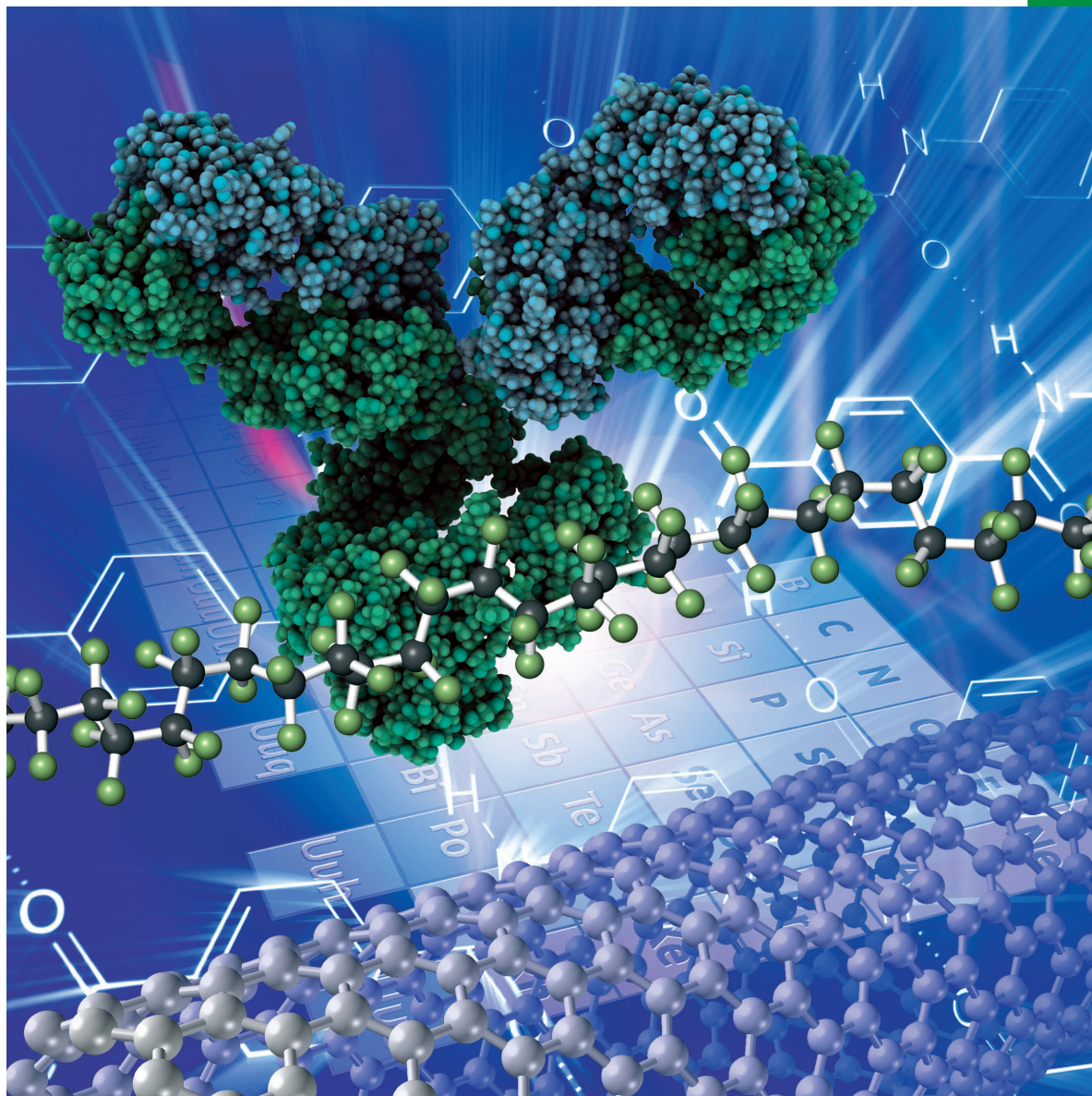
Copyright © 1999-2020 John Wiley & Sons, Inc. All rights reserved

Chemistry *SELECT*



www.chemistryselect.org

A journal of



REPRINT

WILEY-VCH

■ Materials Science inc. Nanomaterials & Polymers

Synthesis of $\text{Sr}_{1+2x}\text{La}_{1-2x}\text{Fe}_{1-x}\text{Nb}_x\text{O}_4$ ($x=0, 0.1, 0.3$, and 0.5) by Sol-gel Method: Structural, Magnetic, and Dielectric Properties

Arif Kurnia,^[a] Emriadi,^[a] Nandang Mufti,^[b] and Zulhadjri*^[a]

One – layered Ruddlesden-Popper phase $\text{Sr}_{1+2x}\text{La}_{1-2x}\text{Fe}_{1-x}\text{Nb}_x\text{O}_4$ doped with niobium was synthesized using a sol-gel method for various Nb concentrations ($x=0, 0.1, 0.3$, and 0.5). Single-phase samples could be observed with $x=0$ and 0.1 , while $x=0.3$ and 0.5 contain additional phases. Microstructure results showed that the increase of niobium content corresponded to a decrease in the grain size of the samples. The magnetic

measurements indicated that antiferromagnetic interactions of doped samples had decreased. The dielectric constant of the samples decreased as x increased due to the increase in conductivity. The origin of conduction in the samples might be caused by hopping conduction due to the mixed oxidation states of iron with charge $+3$ and $+4$.

Introduction

Ruddlesden-Popper (RP) phase materials are interesting as they can be used as superconductor, magnetoresistance, ferroelectric and dielectric materials.^[1,2] They have the general formula $A_{n+1}B_n\text{O}_{3n+1}$ where A is an alkaline, alkaline earth, or rare-earth cation and B is a transition element cation. Generally, this phase is constructed from ABO_3 -perovskite blocks of corner-sharing BO_6 octahedra, these blocks being infinite in-plane xy and having n layers in direction z . A certain number of blocks are separated by AO-rock salt slabs so that the unit formula also can be represented with $\text{AO}(\text{ABO}_3)_n$.^[3] It is well known that the properties of the RP phase depend on the nature and composition of cations at the A - and B -site.^[4–7] As reported in [6], antiferromagnetic interactions in SrLaMnO_4 gradually decrease when strontium is partially substituted by barium. Sr_2TiO_4 , which has been found to have no absorption in the visible light spectrum can intensely absorb in the 400–600 nm range after doping with Fe^{3+} and La^{3+} .^[7]

SrLaFeO_4 is a RP phase material with a K_2NiF_4 -type structure and which has been found to be tetragonal $I4/mmm$ with the lattice parameters of $a \approx 3.87 \text{ \AA}$ and $c \approx 12.7 \text{ \AA}$.^[8] This compound exhibits high ion-electron conductivity, significant oxygen diffusion, thermo-mechanical stability, and can be used in solid oxide fuel cells and as a catalyst.^[8–10] SrLaFeO_4 is semiconducting at room temperature and antiferromagnetic with $T_N = 380 \text{ K}$.^[11]

Many studies have been done on the structure and magnetic properties of SrLaFeO_4 and its doping members.^[9–12] Most of them focus on doping at A -site and have mostly substituted the La^{3+} cation with Ca^{2+} , Sr^{2+} , Ba^{2+} , Nd^{3+} , Gd^{3+} , or Dy^{3+} . On the other hand, doping at B -site in SrLaFeO_4 has not received as much attention. Theoretically, cation disorder could occur due to the difference in ionic radii and valences in B -site perovskite which would affect the properties.^[13–15] In some cases, ferromagnetic interactions increase with substitution of a magnetic cation in a perovskite block by high valence cation.^[16–20] For instance, Chai et al.^[19] and Hideki Taguchi^[20] have reported that $\text{Ca}_4\text{Mn}_3\text{O}_{10}$ and CaMnO_3 that are Nb-doped at B -site have increased Weiss constant with increased doping, indicating an increase in ferromagnetic interactions as the presence of mixed-valence in the magnetic cation is increased. Those results suggest that the doping effect induced by niobium could enhance the magnetic properties of antiferromagnetic SrLaFeO_4 . However, as yet, there appears to be no published study about the effect of niobium doping at this site on SrLaFeO_4 . In general, the presence of different valency ions in B -site has been found to lead to the formation of other phases.^[21] The solid-state method has been used in doping RP containing Fe^{3+} cations with other cations but has resulted in impurities.^[21–23] Furthermore, controlling the homogeneity of the reactants is difficult when conventional solid-state methods are used. However, an alternative method, sol-gel, has recently been reported to result in successful synthesis of an RP phase containing different cations at B -site.^[7] The sol-gel method results in high homogeneity in the mixture of the precursors since they are mixed at the atomic level.^[24] It, therefore, seemed reasonable to attempt to synthesize a perovskite block containing both Fe^{3+} and Nb^{5+} cations in the RP phase by this method.

We performed the substitution of niobium in SrLaFeO_4 according to the formula $\text{Sr}_{1+2x}\text{La}_{1-2x}\text{Fe}_{1-x}\text{Nb}_x\text{O}_4$ ($x=0, 0.1, 0.3$, and 0.5) using sol-gel method. We investigated the structure,

[a] A. Kurnia, Prof. Emriadi, Dr. Zulhadjri
Department of Chemistry, Faculty of Mathematics and Natural Sciences,
Universitas Andalas, Padang 25163, Indonesia
E-mail: zulhadjri@sci.unand.ac.id

[b] Dr. N. Mufti
Department of Physics, Faculty of Mathematics and Natural Sciences,
Universitas Negeri Malang, Malang 65145, Indonesia

Supporting information for this article is available on the WWW under
<https://doi.org/10.1002/slct.201904297>

microstructure, and optical and magnetic properties of the products. In recent years, semiconducting materials based on the RP phase have been developed as giant dielectric materials.^[25] Since there is no information about the dielectric properties for this compound, this will provide useful data. We also investigated ac conductivity to provide information related to the phenomenon of surface conduction and its response to temperature and frequency.

Results and Discussion

The X-ray diffraction (XRD) patterns of $\text{Sr}_{1+2x}\text{La}_{1-2x}\text{Fe}_{1-x}\text{Nb}_x\text{O}_4$ ($x = 0, 0.1, 0.3$ and 0.5) at room temperature are shown in Figure 1.

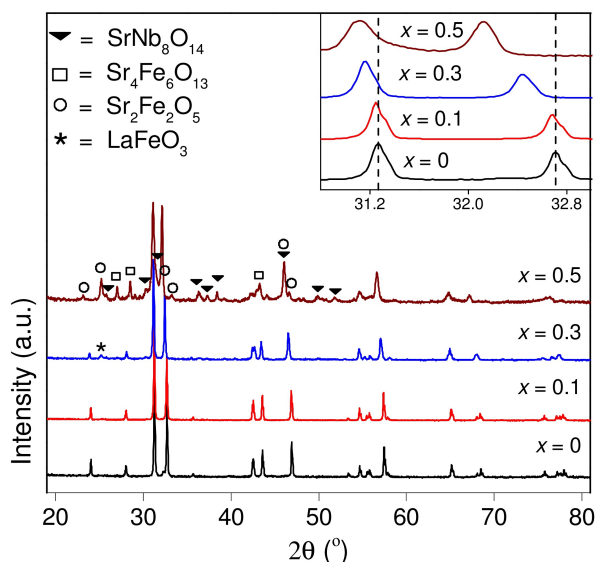


Figure 1. X-ray Diffraction patterns of $\text{Sr}_{1+2x}\text{La}_{1-2x}\text{Fe}_{1-x}\text{Nb}_x\text{O}_4$. Inset: magnification of the main peak upon variation of x .

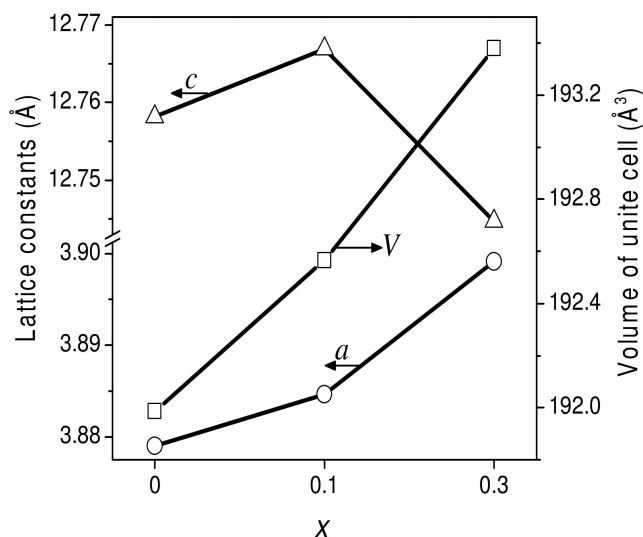


Figure 2. Lattice constants and volume of the unit cell of $\text{Sr}_{1+2x}\text{La}_{1-2x}\text{Fe}_{1-x}\text{Nb}_x\text{O}_4$.

In general, all samples show similar diffraction patterns that can be indexed as a tetragonal $I4/mmm$ space group. No trace of impurity was found at $x=0$ and 0.1 , while a low-intensity peak of perovskite LaFeO_3 can be observed at $x=0.3$. On the other hand, the existence of other phases such as $\text{SrNb}_8\text{O}_{14}$, $\text{Sr}_2\text{Fe}_2\text{O}_5$, and $\text{Sr}_4\text{Fe}_6\text{O}_{13}$ was detected at $x=0.5$. The XRD data indicated that up to 30% molar ratio iron could be substituted partially by niobium in SrLaFeO_4 . Additionally, strontium content increased proportionally to cover the difference in charge between Fe^{3+} and Nb^{5+} with the substitution at B -site. In inset Figure 1, the two main peaks around 31° shifted toward lower 2θ as x increased, corresponding to an increase of unit cell volume according to Vegard's law. The identification of lattice parameters used the structural parameters of SrLaFeO_4 as the starting model.^[9]

The lattice parameters and cell volume of samples are given in Figure 2. The cell volume increases monotonously with x . These results are consistent with the shift in XRD results. As expected, the cell volume increases as the proportion of niobium increased since the ionic radius of Sr^{2+} (1.31 \AA) is larger than La^{3+} (1.216 \AA) for 9-fold coordination, while the ionic radius of Fe^{3+} (0.645 \AA) is nearly the same as Nb^{5+} (0.640 \AA) for 6-fold coordination.

The scanning electron microscopy (SEM) images of the sample after sintering are presented in Figure 3. The sintered samples with $x=0$ are plate-like in shape, and at $x=0.1$ and 0.3 are shaped irregularly. The grain size of samples with $x=0, 0.1$, and 0.3 are $1\text{--}4 \text{ }\mu\text{m}$, $0.3\text{--}1.5 \text{ }\mu\text{m}$, and $100\text{--}700 \text{ nm}$, respectively with grain size decreasing for higher x . This difference indicates that the introduction of niobium restricts grain growth in the samples.^[26,27]

To investigate the electronic structure of $\text{Sr}_{1+2x}\text{La}_{1-2x}\text{Fe}_{1-x}\text{Nb}_x\text{O}_4$ ($x=0, 0.1$, and 0.3) we used the optical absorption spectroscopy. This method has been widely used to study transition metal complexes, including the d^5 system.^[28,29] The Fourier transform of diffuse reflectance spectra of undoped and doped SrLaFeO_4 are shown in Figure S1. A peak for all samples around 1.5 eV attributed to metal $d\text{--}d$ transitions is visible. However, according to the dipole selection rule ($\Delta l = \pm 1$) and the spin selection rule ($\Delta S = 0$), for the case of Fe^{3+} ions in FeO_6 octahedrons, $d\text{--}d$ transitions should be forbidden. The intensity of the spin forbidden $d\text{--}d$ transitions is supposed to be weak.^[28,29] Nevertheless, the $d\text{--}d$ transitions observed for this case are obvious and higher than expected. The reason for the phenomenon might be related to the presence of iron ions with charges of $+2$, $+3$, and $+4$. Tanabe – Sugano (TS) diagrams have been used to predict spin-allowed crystal field of transition peaks for high spin Fe^{2+} and Fe^{4+} , while high spin Fe^{3+} was predicted to have zero spin-allowed transitions.^[28,29] The spin-allowed $d\text{--}d$ transitions for Fe^{2+} ($t_{2g}^4 e_g^2 \rightarrow t_{2g}^3 e_g^3$) and Fe^{4+} ($t_{2g}^3 e_g^1 \rightarrow t_{2g}^2 e_g^2$) were found at the $10Dq$ values 1.277 eV and 1.723 eV , respectively. Warshi et al. have studied the mixed state of Fe from YFeO_3 using XANES and absorption spectroscopy.^[29] However, they could only confirm $d\text{--}d$ transition for the samples with mixed-valence $\text{Fe}^{2+}/\text{Fe}^{3+}$ using XANES, while the peak around 1.277 was not observed in the absorption spectra. On the other hand, the samples containing

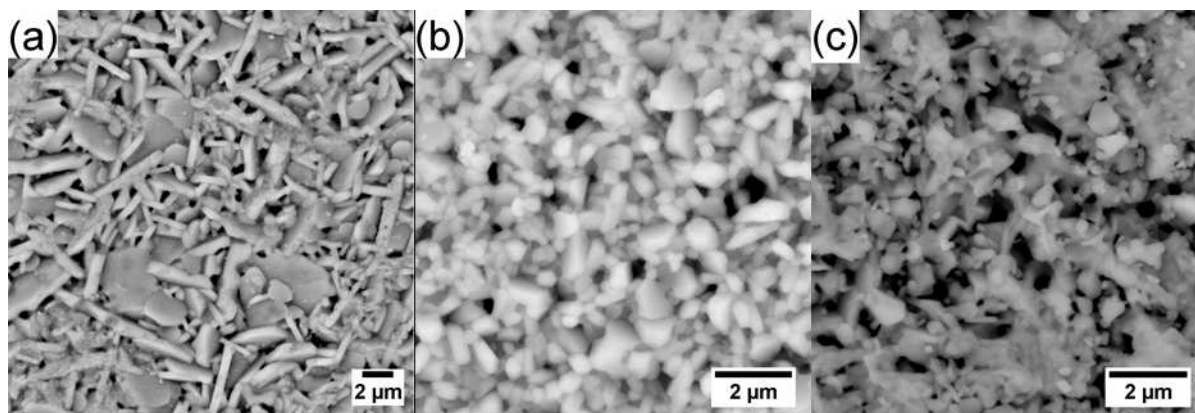


Figure 3. SEM images of $\text{Sr}_{1+2x}\text{La}_{1-2x}\text{Fe}_{1-x}\text{Nb}_x\text{O}_4$. (a) $x=0$, (b) $x=0.1$, (c) $x=0.3$.

iron with charge +3 and +4 could be observed using both instruments. Those results imply that the absorption spectra from our samples could indicate the presence of $\text{Fe}^{3+/4+}$, which is in agreement with other reports.^[30,31]

As the mixed state of iron is +3 and +4 in SrLaFeO_4 , the presence of excess oxygen formation is suggested despite no clear evidence to support it.^[31,32] Unlike in perovskite compounds,^[33,34] Omata et al. proposed the possibility of the incorporation of excess oxygen atoms into the crystalline lattice of SrLaFeO_4 at the interstitial site between adjacent (Sr,La)-O planes which generates positive holes.^[32] However, positive holes were not detected by Mossbauer's experiment due to two factors. First, a positive hole is stabilized by the excess negative charge from filled O2p bands in oxygen. Another factor is the concentration of the positive holes is less than the limit detection of the instrument. Therefore, further study is still needed in this case to investigate that phenomenon.

Figure 4 shows magnetic measurement results of $\text{Sr}_{1+2x}\text{La}_{1-2x}\text{Fe}_{1-x}\text{Nb}_x\text{O}_4$ ceramics. The plots of the temperature dependence of $1/\chi$ (inverse of magnetic susceptibility) at $x=0$ and 0.3 yield the negative Weiss constants (θ) of -300 and -82 K, respectively as shown in Figure 4a. The result indicates that both samples are antiferromagnetic.^[35] However, the value of θ increases for the doped sample, implying that the antiferromagnetic interaction decreases.^[19] The effective magnetic moment (μ_{eff}) at $x=0$ and 0.3 calculated from Currie-Weiss law are found to have the values $5.2 \mu\text{B}$ and $4.6 \mu\text{B}$, respectively. The decrease in the value of μ_{eff} due to doping might be related to the change in the ratio of the iron charge. The μ_{eff} of the sample with $x=0$ is close to the theoretical spin-only moment of Fe^{3+} ($5.92 \mu\text{B}$) indicating the domination of super-exchange antiferromagnetic interactions ($\text{Fe}^{3+}-\text{O}^{2-}-\text{Fe}^{3+}$).^[23,36] The lower value of μ_{eff} at $x=0.3$ could imply the presence of Fe^{4+} or Fe^{2+} increase as both cations have a smaller magnetic moment ($4.9 \mu\text{B}$). In this work, an increase of Fe^{4+} is more reasonable as it is confirmed by absorption spectroscopy measurements. The change of θ and μ_{eff} value with niobium doping may be attributed to the enhancement of double exchange interactions ($\text{Fe}^{3+}-\text{O}^{2-}-\text{Fe}^{4+}$).^[19] Figure 4b displays the magnetic field

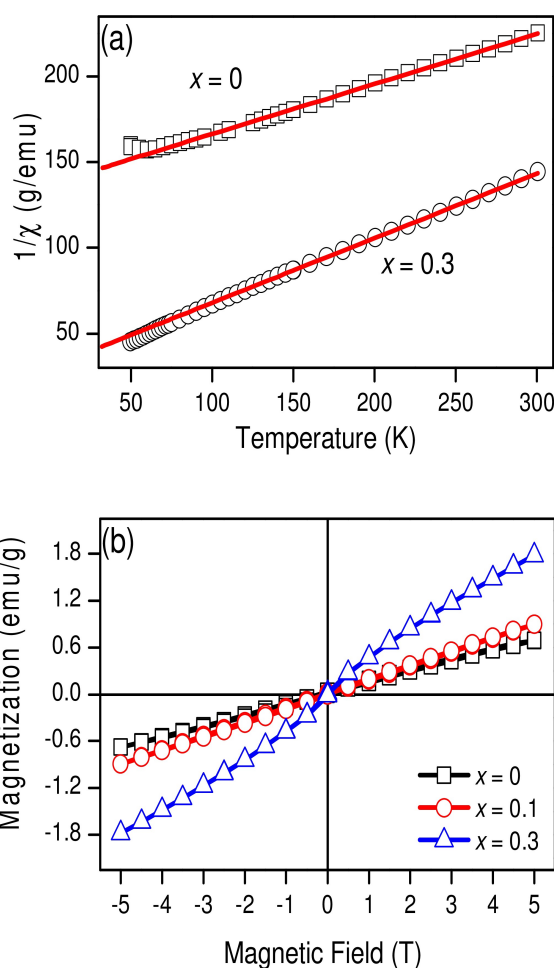


Figure 4. Magnetic measurement results of $\text{Sr}_{1+2x}\text{La}_{1-2x}\text{Fe}_{1-x}\text{Nb}_x\text{O}_4$ ceramics. (a) Temperature dependence of $1/\chi$. (b) Magnetic field dependence of magnetization at 50 K.

dependence of magnetization for samples with $x=0$, 0.1, and 0.3 at $T=50$ K. Magnetization does not saturate up to the available field (5T) with no loop opening, indicating a typical antiferromagnetic interaction. The magnetization increases

noticeably as x increases, which is related to the increase of double exchange interaction in the sample.^[37]

Figure 5 shows the frequency dependence of the dielectric constant (ϵ') for samples with $x=0, 0.1$, and 0.3 which were measured at the selected temperature in the frequency range of 1 kHz to 300 kHz. All samples at selected temperatures exhibit high dielectric constants at low frequency. For example, at 1 kHz and room temperature, the values of dielectric constant for the samples with $x=0, 0.1$, and 0.3 are 1.80×10^4 , 1.58×10^4 , and 1.52×10^4 , respectively. However, at a higher frequency (100 kHz) these values decrease to 1.16×10^4 , $9.91 \times$

10^3 , and 5.29×10^3 . This behavior has been observed in many compounds and has been explained by dipole relaxation in which the dipole is able to follow the low frequencies but unable to follow at higher frequencies.^[25,38–40] Moreover, pores, voids, interstitial and vacancy defects, dislocations, grain boundaries, and dipoles also contribute to dielectric properties in our samples. It can be seen that the value of the dielectric constant decreases as x increases. This may be related to the grain size of samples since larger grains give higher dielectric constants.^[41] The values of the dielectric constant at 1 kHz of this sample are higher than that of $\text{La}_{2-x}\text{Ca}_x\text{NiO}_{4+\delta}$ ($x=0, 0.1, 0.2, 0.3$) that have been measured in previous studies.^[25]

The value of ac conductivity ($\sigma_{ac} = \omega \epsilon \epsilon''$, where $\omega = 2\pi f$ is angular frequency, ϵ is permittivity of free space, and ϵ'' is the imaginary part of the dielectric constant) as a function of frequency for samples with $x=0, 0.1$, and 0.3 reflects similar behavior to the dielectric constant values, as can be seen from Figure 6. Conductivity clearly decreases with decreasing frequency and then becomes nearly constant at a certain frequency. Thus, ac conductivity can be divided into two regions. In the first region, the dc plateau region, conductivity appears to be frequency-independent. The value of conductivity in this region increases as temperature increases, indicating that the conduction process is thermally activated. In the second region, the frequency-dependent region, conductivity increases dramatically with frequency.^[42] For example, at 10 kHz and room temperature, the values of conductivity for the samples with $x=0, 0.1$ and 0.3 are 1.42×10^{-3} , 2.37×10^{-3} , and $3.14 \times 10^{-3} \Omega^{-1}\text{m}^{-1}$, respectively which increase to 3.18×10^{-2} , 3.3×10^{-2} , and $2.04 \times 10^{-2} \Omega^{-1}\text{m}^{-1}$ at 100 kHz. There is also an increase in conductivity when x is increased. This increase in conductivity causes a decrease in the dielectric constant of the samples.

To obtain further information regarding the conduction process, Jonscher's power law, the "universal dielectric response" (UDR), was utilized:

$$\sigma_{ac} = \sigma_{dc} + B\omega^n$$

where σ_{dc} is conductivity at dc plateau region, B is the temperature and material-dependent pre-exponential factor, and n is frequency exponent. The plot at curvature σ_{ac} vs. frequency gives the exponent n . The fitted value of n for all samples was found to be between 0.5 and 1. A value of $0 \leq n \leq 1$ indicates hopping conduction.^[43,44] To differentiate between electrons or polarons as the origin of hopping conduction the activation energy of samples with $x=0, 0.1$, and 0.3 was determined using the Arrhenius equation:

$$\sigma = \sigma_0 \exp(E_a/K_B T)$$

where σ_0 is the pre-exponential term and E_a is the activation energy. The E_a value is extracted from the linear plot of $\log \sigma_{dc}$ vs. temperature (Figure 7). The experimental value of activation energy was found to be 0.092, 0.089, and 0.097 eV for samples with $x=0, 0.1$, and 0.3 , respectively. These values suggest that the hopping conduction is caused by the mixed-valence state

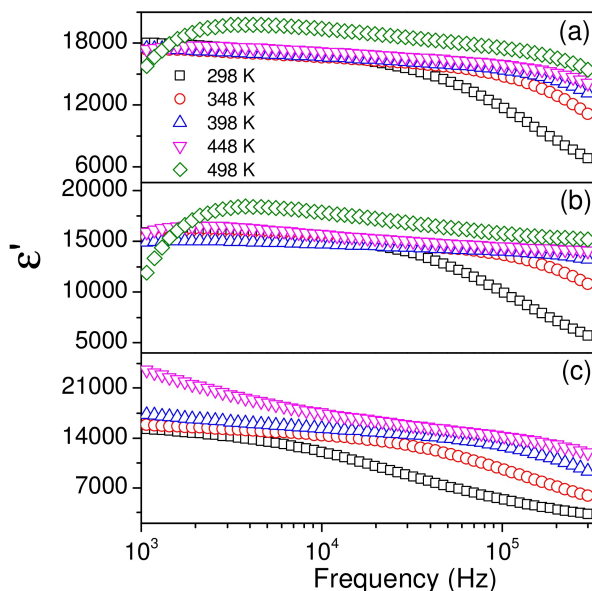


Figure 5. Frequency dependence of dielectric constant of $\text{Sr}_{1+2x}\text{La}_{1-2x}\text{Fe}_{1-x}\text{Nb}_x\text{O}_4$. (a) $x=0$, (b) $x=0.1$, (c) $x=0.3$.

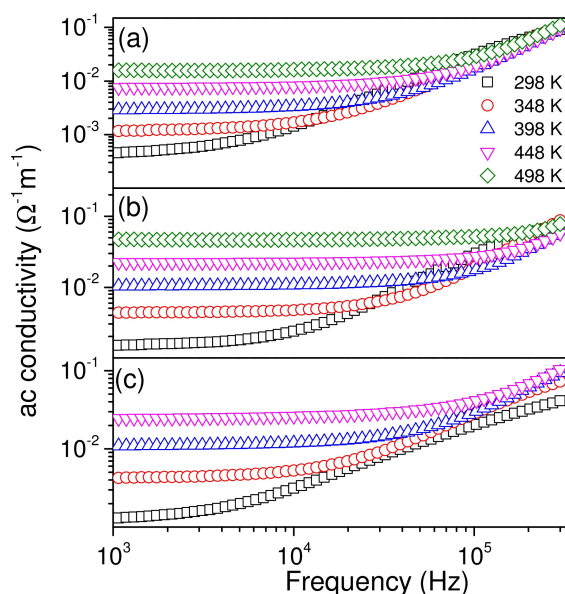


Figure 6. Frequency dependence of ac conductivity of $\text{Sr}_{1+2x}\text{La}_{1-2x}\text{Fe}_{1-x}\text{Nb}_x\text{O}_4$. (a) $x=0$, (b) $x=0.1$, (c) $x=0.3$.

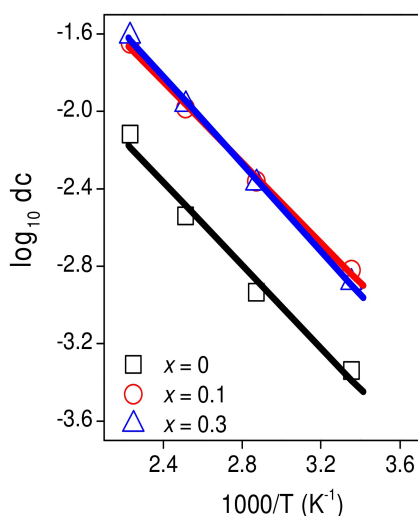


Figure 7. Temperature dependence of dc conductivity of $\text{Sr}_{1+2x}\text{La}_{1-2x}\text{Fe}_{1-x}\text{Nb}_x\text{O}_4$.

of magnetic cations.^[20,44] In this case, hopping conduction is due to the presence of mixed-valence iron.

Conclusions

A one-layered RP compound SrLaFeO_4 has been synthesized by the sol-gel method, with Fe^{3+} partially substituted by Nb^{5+} . Pure RP compounds were found for the samples with $x=0$ and 0.1 , while a small peak of impurity was observed at $x=0.3$. The samples have tetragonal $I4/mmm$ space group symmetry and the cell volume increases as x increases. The grain size of the sample reduces as niobium doping increases. The dielectric constant value of the sample decreases as x increases and is related to the increased conductivity. The conduction process in samples is hopping conduction resulting from the contribution of $\text{Fe}^{3+/4+}$.

Supporting Information Summary

Experimental section and additional data are provided in the Supporting Information.

Acknowledgments

This work was supported by the Ministry of Research, Technology and Higher Education of the Republic of Indonesia for the financial support through the PMDSU Scholarship [Grant number 050/SP2H/LT/DRPM/2018], the PKPI-PMDSU Scholarship [Grant number 1406.53/D3/PG/2018]. The authors acknowledge Dr. Umut Adem for fruitful discussion and thank İzmir Institute of Technology's Center for Materials Research for SEM experiment.

Conflict of Interest

The authors declare no conflict of interest.

Keywords: Ruddlesden-Popper • Sol-gel method • Antiferromagnetic • Dielectric constant • Hopping conduction

- [1] S. Sharma, A. Mahajan, S. Singh, R. Singh, D. Singh, *Ionics (Kiel)*. **2013**, *19*, 505–509.
- [2] X. Q. Liu, J. W. Wu, X. X. Shi, H. J. Zhao, H. Y. Zhou, R. H. Qiu, W. Q. Zhang, X. M. Chen, *Appl. Phys. Lett.* **2015**, *106*, 1–4.
- [3] B. V. Beznosikov, K. S. Aleksandrov, *Crystallogr. Rep.* **2000**, *45*, 864–870.
- [4] H. Nakano, N. Ishizawa, N. Kamegashira, Zulhadjri, T. Shishido, *J. Alloys Compd.* **2006**, *408–412*, 593–597.
- [5] Y. E. Putri, S. M. Said, R. Refinel, M. Ohtaki, S. Syukri, *Electron. Mater. Lett.* **2018**, *14*, 556–562.
- [6] M. Bieringer, J. E. Greedan, *J. Mater. Chem.* **2002**, *12*, 279–287.
- [7] H. Zhang, S. Ni, Y. Mi, X. Xu, *J. Catal.* **2018**, *359*, 112–121.
- [8] H. Chen, X. Sun, X. Xu, *Electrochim. Acta* **2017**, *252*, 138–146.
- [9] S. Gupta, M. K. Verma, D. Singh, *Ceram. Int.* **2016**, *42*, 18418–18424.
- [10] S. Gupta, M. K. Verma, N. D. Sharma, D. Singh, *Polyhedron* **2016**, *122*, 79–85.
- [11] D. Singh, S. Singh, A. Mahajan, N. Choudhary, *Ceram. Int.* **2014**, *40*, 1183–1188.
- [12] S. Fujihara, T. Nakata, H. Kozuka, T. Yoko, *J. Solid State Chem.* **1995**, *115*, 456–463.
- [13] K. I. Doig, J. J. P. Peters, S. Nawaz, D. Walker, M. Walker, M. R. Lees, R. Beanland, A. M. Sanchez, C. F. Mcconville, V. R. Palkar, et al., *Sci. Rep.* **2015**, *5*, 1–10.
- [14] S. B. Majumder, S. Bhattacharyya, R. S. Katiyar, A. Manivannan, P. Dutta, M. S. Sheehra, *J. Appl. Phys.* **2006**, *99*, 1–9.
- [15] B. Schüpp, K. Dörr, K. Ruck, K. Nenkov, K. Müller, G. Krabbes, *Solid State Sci.* **2005**, *7*, 17–23.
- [16] Y. Jun, W. Moon, C. Chang, H. Kim, H. S. Ryu, J. W. Kim, K. H. Kim, S. Hong, *Solid State Commun.* **2005**, *135*, 133–137.
- [17] Y. Jun, S. Hong, *Solid State Commun.* **2007**, *144*, 329–333.
- [18] H. Singh, K. L. Yadav, *Mater. Chem. Phys.* **2012**, *132*, 17–21.
- [19] P. Chai, X. Liu, M. Lu, Z. Wang, J. Meng, *Chem. Mater.* **2008**, *20*, 1988–1996.
- [20] H. Taguchi, *Phys. B Condens. Matter* **2001**, *304*, 38–44.
- [21] A. J. Jennings, S. J. Skinner, O. Helgason, *J. Solid State Chem.* **2004**, *177*, 45–54.
- [22] J. H. Shin, M. S. Song, J. Y. Lee, *J. Electroceram.* **2006**, *17*, 205–209.
- [23] I. B. Sharma, S. Kumari, S. Gupta, *J. Alloys Compd.* **2005**, *402*, 12–16.
- [24] W. Ge, C. Zhu, H. An, Z. Li, G. Tang, D. Hou, *Ceram. Int.* **2014**, *40*, 1569–1574.
- [25] C. Shi, Z. Hu, Y. Hao, *J. Alloys Compd.* **2011**, *509*, 1333–1337.
- [26] T. Wang, T. Xu, S. Gao, S.-H. Song, *Ceram. Int.* **2017**, *45*, 4489–4495.
- [27] M. Hojamberdiev, K. Kawashima, M. Kumar, A. Yamakata, K. Yubuta, A. Gurlo, M. Hasegawa, K. Domen, K. Teshima, *Int. J. Hydrogen Energy* **2017**, *42*, 27024–27033.
- [28] A. Kumar, A. Sati, V. Mishra, M. K. Warshi, R. Kumar, P. R. Sagdeo, *J. Phys. Chem. Solids* **2019**, *135*, 109102.
- [29] M. K. Warshi, A. Kumar, V. Mishra, A. Sati, A. Sagdeo, R. Kumar, P. R. Sagdeo, *J. Appl. Phys.* **2019**, *125*, 1–7.
- [30] A. J. Jennings, S. J. Skinner, *Solid State Ionics* **2002**, *152–153*, 663–667.
- [31] A. J. Jennings, S. J. Skinner, O. Helgason, *J. Solid State Chem.* **2003**, *175*, 207–217.
- [32] T. Omata, K. Ueda, N. Ueda, M. Katada, S. Fujitsu, T. Hashimoto, *Solid State Commun.* **1993**, *88*, 807–811.
- [33] N. I. Solin, S. V. Naumov, N. M. Chebotaev, A. V. Korolev, *Magn. Ferroelectr.* **2010**, *52*, 289–297.
- [34] R. I. Dass, J.-Q. Yan, J. B. Goodenough, *Phys. Rev. B* **2003**, *68*, 1–12.
- [35] Y. Wang, H. Liu, P. Fu, H. Lu, *Sci. China Mater.* **2019**, *62*, 1815–1820.
- [36] H. Lu, T. Yamamoto, W. Yoshimune, N. Hayashi, Y. Kobayashi, Y. Ajiro, H. Kageyama, *J. Am. Chem. Soc.* **2015**, *137*, 9804–9807.
- [37] M. B. Bellakki, V. Manivannan, P. McCurdy, S. Kohli, *J. Rare Earth* **2009**, *27*, 691–697.
- [38] Y. Ma, X. M. Chen, Y. Q. Lin, *J. Appl. Phys.* **2008**, *103*, 1–6.
- [39] M. Kamran, A. Ullah, S. Rahman, A. Tahir, K. Nadeem, M. Anis, S. Hussain, *J. Magn. Magn. Mater.* **2017**, *433*, 178–186.
- [40] S. Huang, L. Shi, Z. Tian, S. Yuan, L. Wang, G. Gong, C. Yin, G. Zehirun, *Ceram. Int.* **2015**, *41*, 691–698.

- [41] V. R. Mudinepalli, L. Feng, W. Lin, B. S. Murty, *J. Advaced Ceram.* **2015**, *4*, 46–53.
- [42] H. Bakkali, M. Dominguez, X. Batlle, A. Labarta, *Sci. Rep.* **2016**, *6*, 1–8.
- [43] Q. Hou, K. Yan, R. Fan, Z. Zhang, M. Chen, K. Sun, C. Cheng, *RSC Adv.* **2015**, *5*, 9472–9475.
- [44] S. Khadhraoui, A. Triki, S. Hcini, S. Zemni, M. Oumezzine, *J. Magn. Magn. Mater.* **2014**, *371*, 69–76.

Submitted: November 11, 2019

Accepted: May 18, 2020